Genome-wide conditional degron libraries for functional genomics

Eduardo Gameiro[1,*], Karla A. Juárez-Núñez [1,*], Jia Jun Fung[1], Susmitha Shankar[1], Brian Luke[1,2,#], Anton Khmelinskii[1,#]

1 Institute of Molecular Biology (IMB), Mainz, Germany
2 Johannes Gutenberg University Mainz, Institute for Developmental Neurology (IDN), Mainz, Germany
* These authors contributed equally
# These authors jointly supervised this work
Correspondence to BL (b.luke@imb-mainz.de) and AK (a.khmelinskii@imb-mainz.de)

Abstract

The yeast knockout library, comprised of strains carrying precise deletions of individual open reading frames (ORFs), has been a vital resource to understand gene function. However, accumulation of suppressor mutations in knockout strains can lead to erroneous functional annotations. Moreover, the library is limited to non-essential ORFs, and must be complemented with hypomorphic alleles of essential ORFs for genome-wide studies. To address these limitations, we constructed genome-wide libraries of conditional alleles based on the auxin-inducible degron (AID) system for conditional degradation of AID-tagged proteins. First, we determined that N-terminal tagging is at least twice more likely to inadvertently impair protein function across the proteome. We thus constructed two genome-wide libraries with over 5600 essential and non-essential proteins fused at the C-terminus with an AID tag and an optional fluorescent protein. Almost 90% of AID-tagged proteins were completely or partially degraded in the presence of auxin, with protein abundance and tag accessibility as limiting factors. Genome-wide screens for DNA damage response factors with the AID libraries revealed a role for the glucose signaling factor *GSF2* in resistance to hydroxyurea, highlighting how these resources extend the toolbox for functional genomics in yeast.

Introduction

Characterization of loss-of-function alleles is the most common approach to study gene function. With its simple genetics and broad range of resources, the budding yeast *Saccharomyces cerevisiae* is an excellent model for functional genomics (Botstein and Fink, 2011). The budding yeast knockout library was the first genome-wide collection of gene deletion strains (Giaever et al., 2002; Winzeler et al., 1999). This resource has enabled hundreds of genome-wide screens for functional profiling of the yeast genome, mapping of genetic interactions, identification of drug targets and mechanisms of drug action (Giaever and Nislow, 2014).

Despite the wide-ranging impact of the yeast knockout library, this resource has some limitations. First, because approximately 20% of yeast genes are essential (Giaever et al., 2002), i.e. their deletion is lethal, the deletion collection should be complemented with conditional alleles of essential genes for complete coverage. Libraries of essential alleles based on transcriptional repression, decreased expression by reducing gene dosage through the use of heterozygous diploids or by mRNA destabilization, temperature sensitivity or targeted protein degradation have been applied with different trade-offs, including variability in the rate and extent of downregulation or side effects of the conditions necessary for downregulation (Ben-Aroya et al., 2008; Breslow et al., 2008; Giaever et al., 2002; Kanemaki et al., 2003; Li et al., 2011; Mnaimneh et al., 2004; Snyder et al., 2019). Another limitation of the knockout library is the masking gene-specific phenotypes by spontaneous suppressor mutations that can arise in gene deletion strains (Van Leeuwen et al., 2016).

Here we sought to address these limitations by developing genome-wide libraries of conditional alleles based on the auxin-inducible degron system AID2 for targeted protein degradation (Nishimura et al., 2009; Yesbolatova et al., 2020). The improved AID2 system allows for tightly controlled and rapid degradation of AID-tagged proteins (Nishimura et al., 2009). We show that nearly complete degradation of most yeast proteins can be achieved with genome-wide AID libraries and demonstrate an application of these resources in genome-wide screens for factors involved in the DNA damage response.

Results

Systematic comparison of N- and C-terminal tagging

We set out to construct genome-wide auxin-inducible degron (AID) libraries, where each strain expresses a different protein fused to the AID tag. To decide at which terminus to fuse the AID tag so that the likelihood of tagging artifacts is minimized, we asked whether protein N- or C-termini are generally more amenable to tagging. Although studies of individual proteins have shown that tagging can impair protein localization or function depending on the tagged terminus, a comprehensive comparison of N- and C-terminal tagging is lacking (Weill et al., 2019).

To systematically assess the relative impact of N- and C-terminal tagging, we established a high-throughput competition assay (Fig. 1a). In this assay, pairs of strains expressing the same protein fused either at the N- or at the C-terminus to a non-fluorescent tag are co-cultured. The frequency of each cell type in the co-cultures is monitored over time by flow cytometry of strain-specific fluorescent markers, the mNeonGreen (mNG) and mCherry fluorescent proteins expressed from a strong constitutive promoter. The relative fitness (α) of the two co-cultured strains is then determined from the change in the relative frequencies of the two cell types over time (Fig. 1a, Methods). Under the assumption that tagging is either neutral or impairs fitness, but is very unlikely to improve fitness, $\alpha < 0$ corresponds to reduced relative fitness of the C-terminally tagged strain and $\alpha > 0$ – reduced relative fitness of the N-terminally tagged one.

We used the high-throughput SWAp-Tag (SWAT) approach (Meurer et al., 2018; Weill et al., 2018; Yofe et al., 2016) to tag open reading frames (ORFs) at endogenous chromosomal loci with a sequence encoding the Halo tag. The SWAT approach makes use of strain arrays with individual ORFs marked with an acceptor module. This module is inserted immediately before the stop codon in C-SWAT strains or after the start codon in N-SWAT strains, except for ORFs encoding proteins with predicted N-terminal signal peptides or N-terminal mitochondrial targeting signals where the acceptor module is placed after the predicted signal sequences. Using semi-automated crossing, the acceptor module can be replaced with practically any tag or regulatory element provided on a donor plasmid (Yofe et al., 2016). Halo tagging using N-SWAT and C-SWAT libraries was efficient, yielding homogeneous strains with over 99% of the cells in most strains expressing the expected fusion protein under control of its native regulatory elements (Fig. S1a, Methods). As the resulting Halo-ORF and ORF-Halo libraries are haploid, the ORF tagged in each strain is the only source of that specific protein.

Next, we competed pairs of matched N- and C-terminally tagged strains and determined the relative fitness impact of the Halo tag location (Fig. 1a). The competition assay yielded reproducible estimates of relative fitness (α) (Fig. S1b). The distribution of relative fitness across all assayed pairs was centered at 0.02 ± 0.17 (mean ± s.d., n = 5247 ORFs) (Fig. 1b, Table S1), suggesting that the impact of the Halo tag was generally independent of the tagged terminus. Importantly, the strain-specific fluorescent markers affected fitness to a similar degree, as indicated by the relative fitness of 0.05 ± 0.01 (mean ± s.d., n = 92 technical replicates) for a pair of untagged strains expressing mNG or mCherry (Fig. S1c). Therefore, the contribution of the fluorescent makers to the detected fitness differences is likely negligeable. Based on these observations, we estimate that fitness differences as low as 5% (corresponding to an absolute $\alpha = 0.175$, Methods) can be measured in the competition assay. Hereafter, ORFs with $\alpha > 0.175$ are referred to as N-losers, with $\alpha < -0.175$ – as C-losers and with absolute $\alpha \leq 0.175$ – as neutral.

Tagging of non-essential ORFs, especially those whose deletion has little to no impact on growth, is unlikely to impair fitness. Accordingly, essential ORFs were more likely to exhibit differential fitness defects in the competition assay (24% compared to 10% of non-essential ORFs) (Fig. 1c). This suggests that up to a quarter of the proteome is differentially affected by terminal tagging, under the assumption that tagging similarly affects essential and non-essential proteins. In addition, tagging at both termini can be detrimental to the function of some proteins. Such cases are likely rare, as no single instance could be detected in triple competition assays for a random set of 45 ORFs, where both tagged variants were competed against the wild type (Fig. S1d, e).

Whereas 155 out of 898 essential ORFs were N-losers, exhibiting reduced relative fitness with N-terminal compared to C-terminal tagging, only 65 essential ORFs were C-losers. This tendency held across the whole dataset, with a total of 434 N-losers and 204 C-losers (Fig. 1b), indicating that N-terminal tagging is more likely to impair protein function compared to C-terminal tagging. Interestingly, the frequency of differential fitness defects varied between subcellular compartments (Fig. 1d). Proteins of the golgi, vacuolar membrane and lipid particle were most likely to be differentially affected by terminal tagging, suggesting that terminal tagging could affect protein localization. Supporting this notion, differential fitness defects correlated with differential localization of N- and C-terminally tagged proteins (Fig. 1e). Using datasets of subcellular localizations for most yeast proteins determined with fluorescence microscopy of strains expressing N- and C-terminal GFP fusions (Breker et al., 2013; Huh et al., 2003; Weill et al., 2018), we observed that for essential genes, only

6% of neutral ORFs exhibited different localizations of N- and C-terminally tagged variants, whereas this fraction increased to 11% and 25% for N-losers and C-losers, respectively. The magnitude of this trend is likely underestimated considering that for 636 proteins the N-terminal Halo tag was not placed at the very N-terminus but after the predicted N-terminal signal peptide or mitochondrial targeting signal, to avoid blocking these localization signals and increase the likelihood of correct protein localization (Yofe et al., 2016). Optimized tagging of proteins with these N-terminal localization signals likely also contributes to the lack of correlation between differential fitness defects and occurrence of terminal localization signals (Fig. S1f, Table S2). Taken together, we conclude that while N-terminal tagging can be beneficial in individual cases, C-terminal tagging is overall less likely to affect protein localization and function.

AID libraries

Based on the above analysis, we constructed genome-wide C-terminally tagged AID libraries. We combined the short AID* tag, which consists of amino acids 71-114 from AtIAA17 (Morawska and Ulrich, 2013; Nishimura et al., 2009), with the AID2 system (Yesbolatova et al., 2020) (Fig. 2a). The AID2 system relies on the OsTir1 F-box protein with the F74G mutation and the auxin analog ligand 5-phenil-indole-3-acetic acid (5-Ph-IAA) to achieve quick and efficient degradation of AID-tagged proteins at significantly lower ligand concentrations than the original AID system and without basal degradation in the absence of 5-Ph-IAA (Nishimura et al., 2009; Yesbolatova et al., 2020). Expression of OsTir1(F74G) from the strong galactose-inducible *GAL1* promoter had a negligeable impact on yeast fitness (Fig. S2a). Using C-SWAT, we tagged each ORF with mNG-AID*-3myc (AID-v1 library, 5604 tagged ORFs) or with AID*-3myc (AID-v2 library, 5620 tagged ORFs) and concomitantly introduced the *GAL1pr-OsTIR1(F74G)* expression construct (Fig. 2b, S2b). The 3myc epitope tag can be used to determine protein levels with immunoblotting, whereas the mNG tag in the AID-v1 library allows assessing protein levels with fluorescence measurements. Whereas all strains in the AID-v2 library carry the *OsTIR1* construct, the AID-v1 library comprises two strains for each ORF, with or without *OsTIR1* (*OsTIR1*$^+$ and *OsTIR1*$^-$, respectively) (Fig. 2b).

We assessed the frequency and the extent of AID-dependent degradation across the proteome using mNG fluorescence in the AID-v1 library. Strains were grown as ordered colony arrays on agar plates with galactose and 5-Ph-IAA, and their fluorescence was measured with a plate reader to determine the levels of mNG-AID*-3myc-tagged proteins (Fig. 2c, Methods). Protein expression levels in *OsTIR1*$^-$ strains correlated well with independent estimates of protein abundance (Meurer et al., 2018) (Fig. S2c, d), indicating that the AID* tag has little impact on protein levels in the absence of the cognate F-box protein. Notably, out of 5079 proteins detected in *OsTIR1*$^-$ strains, 4455 (~88%) were significantly depleted in *OsTIR1*$^+$ strains (Fig. 2d, Table S3). 3981 proteins could not be detected specifically in the *OsTIR1*$^+$ background, suggesting their complete degradation by the AID system, and 474 proteins were partially degraded. The fraction of conditionally-degraded proteins (completely or partially degraded) varied with their subcellular localization, and was lowest for proteins localized to membrane-bound organelles such as mitochondria, vacuole, Golgi and endoplasmic reticulum (ER) (Fig. 2e), likely due to inaccessibility of the AID* tag to the cytosolic OsTir1. Supporting this notion, membrane proteins with cytosolic C-termini were more likely to be conditionally degraded compared to those with lumenal or extracellular C-termini (Kim et al., 2006) (Fig. 2e). Finally, the extent of AID-dependent degradation varied with protein abundance, in that highly expressed proteins were more likely to be only partially degraded compared to lowly expressed ones (Fig. 2e, Fig. S2e), suggesting saturation of the AID machinery. It remains to be determined whether OsTir1 or the yeast subunits of the SCF ubiquitin ligase are limiting factors for complete degradation of abundant proteins.

We asked whether AID-dependent protein degradation results in cellular phenotypes. For that, we measured colony sizes in the arrayed AID-v1 library as a readout of strain fitness (Fig. 2c, Methods). In total, ~15% of *OsTIR1*$^+$ strains (820 out of 5604) exhibited impaired fitness compared to *OsTIR1*$^-$ strains (Fig. 3a, Table S3). As expected, the frequency of fitness defects was higher for essential proteins. Whereas fitness defects were observed for over 60% of essential ORFs (547 out of 906), only ~6% of *OsTIR1*$^+$ strains for non-essential ORFs (273 out of 4698) had fitness defects (Fig. 3b). A similar frequency was previously observed with a set of AID alleles constructed for 758 essential ORFs using the original AID system (Snyder et al., 2019). However, over a third of these alleles exhibited fitness defects even in the absence of auxin, which were further compounded by off-target effects of auxin, highlighting the advantages of the AID2 system.

Importantly, the frequency of fitness defects in the AID-v1 library correlated with the extent of protein degradation. Whereas complete degradation resulted in a fitness defect for over 67% of essential proteins, this fraction dropped to 27% and 9% of essential proteins that are partially degraded or not degraded in an AID-dependent manner, respectively (Fig. 3c). Interestingly, complete degradation of 33% of essential proteins did not result in a fitness defect. It is possible that in some cases partial degradation results in low protein levels that are below the detection limit of our assay but are sufficient for viability. In addition, it is likely that

the fraction of strains with the complete degradation phenotype is overestimated in our analysis as colony fluorescence usually scales with colony size, which would result in underestimated fluorescence levels for strains with fitness defects (Fung et al., 2022). Indeed, *OsTIR1*$^{+}$ strains with impaired fitness typically exhibited fluorescence levels below background autofluorescence (Fig. S3a, b). Nevertheless, the frequency of fitness defects depended on the accessibility of the tag and the abundance of the tagged proteins (Fig. 3d), in agreement with the analysis of the degradation extent (Fig. 2e). Thus, while the likelihood and the extent of conditional protein degradation in the AID libraries depend on the abundance of the target protein and the accessibility of the AID tag, most yeast proteins can be efficiently degraded with the AID system, resulting in cellular phenotypes consistent with loss of the target protein.

Screens for DNA damage response factors

We sought to apply the AID libraries to screen for factors involved in the DNA damage response using sensitivity to genotoxic agents as a phenotypic readout. We decided to use the DNA damaging agent methyl methanesulfonate (MMS), the topoisomerase I inhibitor camptothecin (CPT) and the ribonucleotide reductase inhibitor hydroxyurea (HU) as genotoxic agents and the AID-v2 library, reasoning that an overall smaller tag (without the mNG moiety) is less likely to inadvertently affect protein function. The library was grown as ordered colony arrays on galactose media with 5-Ph-IAA, a genotoxic agent or both compounds (Fig. 4a). First, we observed that treatment of the AID-v2 library with 5-Ph-IAA resulted in fitness defects consistent with the AID-v1 library (spearman correlation coefficient $\rho = 0.6$, Fig. S4a). These fitness defects similarly correlated with protein essentiality, expression levels, tag accessibility and extent of AID-dependent degradation (Fig. S4b-e), indicating that the AID-v1 and AID-v2 libraries perform comparably.

Next, we calculated chemical-genetic interaction (CGI) scores between each AID allele and a genotoxic agent (Fig. S5a). We focused on negative CGIs whereby the double perturbation (5-Ph-IAA and genotoxic agent) results in a stronger fitness defect than expected from the combined effects of the single perturbations (Methods) (Baryshnikova et al., 2010b; Parsons et al., 2003). This led to the identification of 93, 32 and 93 potential resistance factors (CGI score ≤ -0.2 and p-value < 0.05) for MMS, CPT and HU, respectively (Fig. 4b, Table S4). There was substantial overlap between the non-essential factors identified here and previous screens with the yeast knockout library (Fig. S5b) (Chang et al., 2002; Parsons et al., 2003). Nevertheless, AID alleles of most resistance factors identified with knockout strains were not sensitive to the corresponding genotoxic agents. We asked whether these factors might not be degraded in the respective AID strains. However, the frequency of ORFs with complete AID-dependent degradation was similar for screen-specific and shared resistance factors (Fig. S5b). Differences in growth conditions and definitions of significant fitness defects likely account for the screen-specific CGIs. Taken together, these results validate the screening approach with AID libraries.

Although the three genotoxic agents act through distinct mechanisms, all can result in the accumulation of DNA double strand breaks (DSBs) (Li et al., 2017; Singh and Xu, 2016; Wyatt and Pittman, 2006). Accordingly, shared resistance factors for MMS, CPT and HU included most members of the *RAD52* epistasis group (Fig. 4b, c), which are involved in repair of DSBs (Game and Mortimer, 1974; Resnick, 1969; Symington, 2002). Moreover, most of the identified resistance factors were associated with gene ontology terms related to DNA damage response, transcription, chromatin organization and cell cycle (Fig. 4d, Fig. S5c, Methods). Notably, whereas CPT- and MMS-specific factors were enriched in genes associated with cell cycle progression, DNA damage response and transcription, HU-specific factors were enriched in components of the endomembrane system, including proteins of the endoplasmic reticulum (ER) and components of endosomal sorting complexes required for transport (ESCRT) (Fig. 4d, Fig. S5c, Table S5). This suggest that HU impairs proliferation through multiple mechanisms, consistent with prior reports (Huang et al., 2016; Kuong and Kuzminov, 2009; Musiałek and Rybaczek, 2021; Takano and Nakatsukasa, 2023).

Finally, we examined *GSF2*, one of the HU-specific resistance factors identified in the screen (Fig. 4d, Fig. S5c). Gsf2 is an integral membrane protein localized to the ER that is involved in biogenesis and export of the hexose transporter Hxt1 from the ER (Sherwood and Carlson, 1999). We confirmed that the *GSF2-AID** strain from the AID-v2 library is sensitive to HU specifically in the presence of 5-Ph-IAA (Fig. 4e). A *gsf2*Δ mutant from the haploid yeast knockout library (Giaever et al., 2002; Winzeler et al., 1999) was not sensitive to HU. In contrast, a *gsf2*Δ strain generated by sporulation of a heterozygous diploid knockout exhibited HU sensitivity similar to the *GSF2-AID** strain (Fig. 4e). This suggests that additional mutations acquired by the knockout library strain are masking the HU sensitivity phenotype. Interestingly, conditional degradation of Gsf2 or knockout of GSF2 did not prevent yeast cells from arresting in early S-phase in response to HU (Fig. 4f). Thus, *GSF2* appears to play no role in the activation of the DNA replication checkpoint and the mechanisms underlying HU sensitivity of *gsf2* mutants remain to be determined.

In conclusion, our work establishes genome-wide libraries of conditional auxin-inducible degron alleles in budding yeast. We demonstrate how these resources can be applied to uncover gene functions, thus adding to the toolkit for functional genomics in this organism (Botstein and Fink, 2011). While the extent of protein degradation in the AID libraries can be assessed in high-throughput with mNG fluorescence, the optional nature of the mNG moiety expands the scope of potential applications. The AID-v2 library should be ideal for high-content fluorescence microscopy screens, where the mNG moiety could otherwise limit screen design. Finally, it is noteworthy that a molecular glue for a ubiquitin ligase located in the cytosol can be used to promote degradation of the vast majority of yeast proteins, including integral membrane proteins. This suggests that targeted protein degraders such as proteolysis-targeting chimeras (PROTACs) could in principle be designed for most proteins relevant in clinical or agricultural applications based on one or a few cytosolic ubiquitin ligases (Békés et al., 2022).

Methods

Yeast strains and growth conditions

All yeast strains used in this work are listed in Table S6 and are derivatives of BY4741, Y8205 or Y7092, ESM356-1, or PJ69-4A. All plasmids used in this work are listed in Table S7. Yeast genome manipulations (gene tagging and gene deletion) were performed using PCR targeting and lithium acetate transformation (Janke et al., 2004; Knop et al., 1999). High-throughput N-terminal and C-terminal tagging were performed with the SWAp-Tag approach using the N-SWAT (Weill et al., 2018) and C-SWAT (Meurer et al., 2018) libraries, respectively, as detailed below. Unless stated otherwise, yeast strains were grown at 30°C with 2% (w/v) glucose as carbon source.

Constructions of Halo libraries

To construct the Halo-ORF library, the donor plasmid pSD-N1-HaloTag-3myc was transformed into the donor strain yKBJ0201. The resulting strain yKBJ0203 was crossed with the N-SWAT library. In addition, to test the efficiency of tagging, the donor strain yMaM1205 was transformed with the donor plasmid pSD-N1-mNeonGreen and crossed with 13 N-SWAT strains for highly expressed proteins.

To construct the ORF-Halo library, the donor plasmid pRS41K-3myc-HaloTag was transformed into the donor strain yKBJ0200. The resulting strain yKBJ0202 was crossed with the C-SWAT library. In addition, to test the efficiency of tagging, the donor strain yKBJ0147 was transformed with the donor plasmid pRS41K-mNeonGreen and crossed with 13 N-SWAT strains for highly expressed proteins.

Crossing and subsequent tagging were performed by sequentially pinning the strains on appropriate media using a pinning robot (Rotor, Singer Instruments) in 384-colony format according to the synthetic genetic array (SGA) procedure (Baryshnikova et al., 2010a; Meurer et al., 2018; Tong et al., 2001) as follows:

- N-SWAT and C-SWAT libraries were assembled in 384-colony format on SC-Ura plates (6.7 g/l yeast nitrogen base without amino acids (BD Biosciences, 291940), 2 g/l amino synthetic complete acid mix lacking uracil (SC-Ura), 20 g/l glucose (Merck, 108337), 20 g/l agar (BD Biosciences, 214010)), whereas donor strains with the appropriate donor plasmids were pinned onto YPD+G418 plates (10 g/l yeast extract (BD Biosciences, 212750), 20 g/l peptone (BD Biosciences, 211677), 20 g/l glucose, 20 g/l agar, 200 mg/l G-418 (Biochrom, A291–25), and grown for 1-2 days at 30°C;

- mating of N-SWAT/C-SWAT and donor strains on YPD plates, 1 day at 30 °C;

- selection of diploids twice on SC(MSG)-Ura + G-418 plates (1.7 g/l yeast nitrogen base without amino acids and ammonium sulfate (BD Biosciences, 233520), 1 g/l monosodium glutamic acid (MSG) (Sigma-Aldrich, G1626), 2 g/l amino acid mix SC(MSG)-Ura (glutamic acid replaced by MSG), 200 mg/l G-418, 20 g/l glucose, 20 g/l agar), 1 day at 30°C;

- sporulation on SPO plates (20 g/l potassium acetate (Sigma-Aldrich, 25059), 20g/l agar), 5-7 days at 23°C;

- selection of haploids, step 1, on SC(MSG)-Leu/Arg/Lys/Ura + canavanine/thialysine plates (50 mg/l canavanine (Sigma-Aldrich, C1625), 50 mg/l thialysine (Sigma-Aldrich, A2636)), 2 days at 30°C;

- selection of haploids, step 2, on SC(MSG)-Leu/Arg/Lys/Ura + canavanine/thialysine/G-418 plates (50 mg/l canavanine, 50 mg/l thialysine, 200 mg/l G-418), 2 days at 30°C;

- selection of haploids, step 3, on SC(MSG)-Leu/Arg/Lys/Ura + canavanine/thialysine/G-418/clonNAT plates (50 mg/l canavanine, 50 mg/l thialysine, 200 mg/l G-418, 100 mg/l clonNAT (Werner BioAgents, 5.0)), 2 days at 30°C. This step was omitted for the cross used to assess tagging efficiency with N-SWAT strains;

- selection of haploids, step 4, on SC(MSG)-Leu/Arg/Lys/Ura + canavanine/thialysine/G-418/clonNAT/hygromycin plates (50 mg/l canavanine, 50 mg/l thialysine, 200 mg/l G-418, 100 mg/l clonNAT, 200 mg/l hygromycin (ant-hg-5, Invivogen), 2 days at 30°C. This step was omitted for the crosses used to assess tagging efficiency with N-SWAT and C-SWAT strains;

- induction of tagging twice on SC-Leu Raf/Gal plates (20 g/l galactose (Serva, 22020) and 20 g/l raffinose (Sigma-Aldrich, R0250) instead of glucose), 2 days at 30°C;

- selection against the acceptor module twice on SC-Leu + 5-FOA plates (1 g/l 5-FOA (Apollo Scientific, PC4054)), 2 days at 30°C;

Finally, the resulting strains were pinned on SC-Leu+Ade plates (300 mg/l adenine (A8626, Sigma-Aldrich)) and grown for 1 day at 30°C before proceeding with fluorescence measurements using flow cytometry and storing the libraries as glycerol stocks at -80°C.

Constructions of AID libraries

To construct the AID-v1 library, the donor plasmid pRS41K-mNeonGreen-AID*-3myc was transformed into the donor strains yEG222 (carrying the GAL1pr-OsTIR1(F74G)-natMX construct) and yMaM1205. To construct the AID-v2 library, the donor plasmid pRS41K-AID*-3myc was transformed into the donor strain yEG222. The resulting strains were crossed with the C-SWAT library. In addition, to test the efficiency of tagging, the donor strain yEG222 was transformed with the donor plasmid pRS41K-mCherry-mNeonGreen and crossed with 13 C-SWAT strains for highly expressed proteins.

Crossing and subsequent tagging were performed by sequentially pinning the strains on appropriate media in 384-colony format using the same procedure as for the Halo libraries with the following changes:

- selection of diploids twice on SC(MSG)-Ura + G-418/clonNAT plates, 1 day at 30°C;

- selection of haploids, step 1, on SC(MSG)-Leu/Arg/Lys/Ura + canavanine/ thialysine/G-418 plates, 2 days at 30°C;

- selection of haploids, step 2, on SC(MSG)-Leu/Arg/Lys/Ura + canavanine/ thialysine/G-418/clonNAT plates, 2 days at 30°C. This step was omitted for the cross used to assess tagging efficiency with the pRS41K-mCherry-mNeonGreen donor plasmid;

- induction of tagging twice on SC-Leu Raf/Gal plates (20 g/l galactose (Serva, 22020) and 20 g/l raffinose (Sigma-Aldrich, R0250) instead of glucose), 2 days at 30°C;

• selection against the acceptor module twice on SC-Leu + 5-FOA plates (1 g/l 5-FOA (Apollo Scientific, PC4054)), 2 days at 30°C;

- selection of successful tagging events with reconstitution of the hygromycin selection marker (after induction of tagging and selection against the acceptor module) twice on SC(MSG)-Leu + hygromycin/clonNAT plates (400 mg/l hygromycin, 100 mg/l clonNAT), 2 days at 30°C.

The same procedure but without clonNAT was used to construct the AID-v1 library without the GAL1pr-OsTIR1(F74G)-natMX construct.

Competition assay

Using a pinning robot, strains from the Halo-ORF and ORF-Halo libraries were co-inoculated in 96-well plates (83.3924.005, Sarstedt) with 200 µl of SC-Leu+Ade medium per well. Each well received the two strains for a given ORF, one N-terminally tagged and carrying a cytosolic mNeonGreen marker and another C-terminally tagged and carrying a cytosolic mCherry marker. Three control wells (1 – non-fluorescent strain yMaM1205, 2 – mCherry-positive donor yKBJ0202, 3 – mNeonGreen-positive donor yKBJ0203, Table S6) served to set the gates for mCherry+ and mNG+ cells per plate. The plates were sealed with air-permeable seals (4ti-0517, 4Titude) and the co-cultures were grown overnight at 30°C to saturation.

Saturated co-cultures were diluted (5 µl of co-culture into 195 µl of SC-Leu+Ade medium) and grown for 4h at 30°C in sealed plates before single-cell fluorescence measurements with flow cytometry corresponding to day 0. After the measurements, the plates with the remaining 175 µl of co-culture per well were sealed and incubated for 20h at 30°C. The procedure starting with dilution of co-cultures was then repeated 3 times (flow cytometry analysis corresponding to days 1-3, 24h interval between measurements).

Triple competition experiments for 45 ORFs selected at random were conducted using the same procedure. Single clones of Halo-ORF and ORF-Halo strains were validated by immunoblotting of whole-cell extracts with anti-myc antibodies (mouse monoclonal, clone 9E10). Matching Halo-ORF and ORF-Halo strains were grown in each well together with a wild type strain lacking fluorescent markers (yMaM1205, Table S6).

Flow cytometry

Strains were inoculated in 96-well plates (83.3924.005, Sarstedt) with 150-200 µl of SC-Leu+Ade medium per well and grown overnight at 30°C to saturation. Saturated cultures were diluted into fresh medium and grown at 30°C for 6 h to 6-8x10^6 cells/ml. Assessment of tagging efficiency during construction of Halo libraries and the high-throughput competition assays were performed with strains grown in SC-Leu+Ade medium.

Single-cell fluorescence intensities were measured on a LSRFortessa SORP flow cytometer (BD Biosciences) using the BD FACSDiva v9.0.1 acquisition software, a 561 nm laser for mCherry excitation, a 600 nm long pass mirror and a 610/20 nm band pass filter for mCherry detection, a 488 nm laser for mNeonGreen excitation, a 505 nm long pass mirror and a 530/30nm band pass filter for mNeonGreen detection and an auto-sampler for microtiter plates in the high-throughput (HTS) mode with the following setting: sample flow rate of

0.5 µl/s, sample volume of 25 µl, mixing volume of 100 µl, mixing speed of 100 µl/s, number of mixes equal to 3 and wash volume of 800 µl. 10000 cells were measured per strain. Measurements were gated for single cells with mCherry or mNeonGreen fluorescence intensities above the maximum intensity of a non-fluorescent control strain (mCherry$^+$ or mNeonGreen$^+$ cells). In the triple competition assay, measurements were additionally gated for cells lacking a fluorescent marker (wild type cells).

Analysis of competition experiments

Data analysis and visualization were performed using custom scripts in R (R Core Team, 2020). Ratios of mNG$^+$/mCherry$^+$ cells were calculated for each well and time point from single cell fluorescence measurements obtained with flow cytometry. For each well, cell count ratios were normalized to time point zero. The relative fitness of the two strains in a well was then determined as the slope α of a linear fit to ln(normalized cell count ratio) over time, with intercept set to zero. Triple competition experiments were analyzed following the same procedure for three cell count ratios: mNG$^+$/mCherry$^+$ cells, mNG$^+$/wild type cells and mCherry$^+$/wild type cells.

Using optical density measurements at 600 nm of fifteen wells, we estimated an average doubling time of 4.5 ± 0.1h (mean ± s.d., n = 15 random ORFs) in the competition assay. The average doubling time allowed translating the relative fitness α into a difference in doubling time under the assumptions that, for a given protein, tagging of only one of the termini affects fitness and that $\alpha \neq 0$ reflects impaired fitness, not improved fitness, of one of the competing strain. Based on this and on estimates of reproducibility and technical noise in the competition assay (Fig. S1a, b), further analysis of differential fitness relied on two thresholds of abs(α) = 0.175 and 0.611 corresponding to 5% and 20% longer doubling time for one of the competing strains.

The annotation of yeast genes as essential or non-essential under standard laboratory growth conditions (Després et al., 2020; Giaever et al., 2002; Winzeler et al., 1999) and a proteome-wide localization dataset of C-terminally GFP-tagged proteins (Huh et al., 2003) were used to stratify the genome-wide distribution of relative fitness (Fig. 1c). Proteins assigned to multiple localization classes where counted in each class.

The relationship between differential localization and differential fitness of N- and C-terminally tagged proteins was examined using proteome-wide localization datasets of N-terminally GFP-tagged proteins expressed from endogenous promoters and of C-terminally GFP-tagged proteins (Huh et al., 2003; Weill et al., 2018). The localization classes *missing*, *ambiguous* and *below threshold* were excluded from the analysis and only proteins with annotated localization in both datasets were considered. N- and C-terminally tagged variants assigned to multiple localization classes were considered to have the same localization if they shared at least one localization assignment (Weill et al., 2018).

The relationship between terminal localization signals and differential fitness of N- and C-terminally tagged strains was examined using a list of 998 validated or predicted localization signals obtained through literature curation or retrieved from the UniProt database (Bateman et al., 2023) (Table S2). The list consists of proteins with a glycosylphosphatidylinositol (GPI) anchor (De Groot et al., 2003; Gíslason et al., 2021), tail-anchored (TA) proteins (Beilharz et al., 2003; Burri and Lithgow, 2004; Lewis and Pelham, 2002; Schuldiner et al., 2008; Šimočková et al., 2008), proteins with a cysteine-rich transmembrane module (CYSTM) (Giolito et al., 2024; Venancio and Aravind, 2010; Zvonarev et al., 2023), acylated proteins (UniProt as of 19.02.2024, search for proteins with lipidation, including N-myristoylation, palmitoylation, GPI-anchor addition and prenylation), proteins with a PTS1 peroxisomal targeting signal (Nötzel et al., 2016) (UniProt as of 24.04.2024, search for proteins with motif: microbody targeting signal, C-terminal peroxisome targeting signal (PTS1), peroxisome targeting signal (PTS1), SKL peroxisome targeting motif, peroxisomal target signal 1 (PTS1) or peroxisomal targeting signal type 1), proteins with a signal peptide (SP) or a mitochondrial targeting signal (MTS) (Somashekara and Muniyappa, 2022; Weill et al., 2018; Yofe et al., 2016), proteins with nuclear localization signals (Bordonné, 2000; Hahn et al., 2008; Lee et al., 2023; Somashekara and Muniyappa, 2022) and proteins with HDEL, KKXX or KXKXX motifs identified by pattern match or retrieved from Uniprot (UniProt as of 24.04.2024, search for proteins with motif: prevents secretion from ER or di-lysine motif).

Colony fluorescence measurements and analysis

The AID-v1 library was assembled in 1536-colony format on SC(MSG)-Leu+Ade Raf/Gal + hygromycin plates using a pinning robot (Rotor, Singer Instruments). For each ORF, six technical replicates of the *OsTIR1*$^+$ strain, three technical replicates of the *OsTIR1*$^-$ strain, three technical replicates of a non-fluorescent strain for background correction (AID-v2_HIS4, Table S6) and four technical replicates of an mNG$^+$ reference strain (AID-v1_OsTIR1$^-$_PDC1, Table S6) were arranged in a 4x4 group (Fig. 2c).

Colony arrays were grown for 24h at 30°C and their fluorescence was measured with a multimode microplate reader equipped with monochromators for precise selection of excitation and emission wavelengths (Spark, Tecan) and a custom temperature-controlled incubation chamber. mNG fluorescence intensities were

measured with 506/5 nm excitation, 524/5 nm emission, 40 µs integration time and two detector gains for optimal detection of proteins across the full range of expression levels in the experiment. In addition, the plates were photographed with a colony imager (Phenobooth, Singer Instruments) to assess strain fitness based on colony size, as detailed in the next section.

Data analysis and visualization were performed using custom scripts in R (R Core Team, 2020). Measurements at the two detector gains were interpolated and consolidated into a single value per colony. For each ORF, measurements were normalized by the average of the reference colonies in the 4x4 group, to correct for spatial and plate effects. Sample measurements were further corrected for background fluorescence (mNG-bkg), by subtraction of the mean of the non-fluorescent colonies in the 4x4 group, or expressed in units of background fluorescence (mNG/bkg), by dividing by the mean of the non-fluorescent colonies in the group, and summarized by the mean and standard deviation of *OsTIR1*$^+$ or *OsTIR1*$^-$ replicates.

Background-corrected intensities of *OsTIR1*$^+$ or *OsTIR1*$^-$ strains were compared with a two-sided t-test and p-values were adjusted for multiple testing using the Benjamini-Hochberg method. mNeonGreen-AID*-3myc-tagged proteins were subsequently classified based on their expression levels and the extent of *OsTIR1*-dependent degradation as follows:

- not detected: mNG/bkg(*OsTIR1*$^-$) ≤ 1.2;
- completely degraded: mNG/bkg(*OsTIR1*$^-$) > 1.2, mNG/bkg(*OsTIR1*$^+$) ≤ 1.2, mNG-bkg(*OsTIR1*$^+$) / mNG-bkg(*OsTIR1*$^-$) < 0.5 and p-value < 0.05;
- partially degraded: mNG/bkg(*OsTIR1*$^-$) > 1.2, mNG/bkg(*OsTIR1*$^+$) > 1.2, mNG-bkg(*OsTIR1*$^+$) / mNG-bkg(*OsTIR1*$^-$) < 0.5 and p-value < 0.05);
- not affected: mNG/bkg(*OsTIR1*$^-$) > 1.2, mNG-bkg(*OsTIR1*$^+$) / mNG-bkg(*OsTIR1*$^-$) ≥ 0.5 or mNG/bkg(*OsTIR1*$^-$) > 1.2, p-value ≥ 0.05.

Background-corrected intensities of *OsTIR1*$^-$ strains were compared to previous fluorescence measurements of a library of mNG-tagged ORFs (mNG-II library) (Meurer et al., 2018). Furthermore, proteins detected in the *OsTIR1*$^-$ background were split into five abundance bins of equal width based on background-corrected mNG intensities (Fig. S2d). The annotation of yeast genes as essential or non-essential under standard laboratory growth conditions (Després et al., 2020; Giaever et al., 2002; Winzeler et al., 1999), a proteome-wide localization dataset of C-terminally GFP-tagged proteins (Huh et al., 2003) and a dataset of membrane protein topology (Kim et al., 2006) were used to further stratify the categorized (according to expression, extent of *OsTIR1*-dependent degradation or *OsTIR1*-dependent fitness impairment) proteins (Fig. 2e, 3d, Fig. S4d).

Arrayed fitness screens and analysis

The AID-v2 library was assembled in 1536-colony format on SC(MSG)-Leu + hygromycin/clonNAT plates using a pinning robot (Rotor, Singer Instruments), with four technical replicates per strain placed next to each other in a 2x2 group. After 24h of growth, the colony arrays were pinned on different media with 5-Ph-IAA and genotoxic agents (GAs): control (YP Raf/Gal + hygromycin/clonNat), 5-Ph-IAA (YP Raf/Gal + hygromycin/clonNat/5-Ph-IAA), GA (YP Raf/Gal + hygromycin/clonNat/GA) and 5-Ph-IAA + GA (YP Raf/Gal + hygromycin/clonNat/5-Ph-IAA/GA) plates, where GA stands for camptothecin (CPT, 250 µM; 7689-03-4, Sigma-Aldrich), hydroxyurea (HU, 150 mM; 127-07-1, Sigma-Aldrich) or methyl methanosulfonate (MMS, 0.02% v/v; 66-27-3, Sigma-Aldrich).

Colony arrays were grown at 30°C and photographed after 24h and 48h with a colony imager (Phenobooth, Singer Instruments). Subsequent data analysis and visualization were performed using custom scripts in R (R Core Team, 2020). The gitter package was used to segment the photographs and determine colony sizes (Wagih and Parts, 2014). The SGA tools package was used to correct for spatial and plate effects (Wagih et al., 2013): four outer rows and columns of dummy colonies on each plate were removed; spatial correction was performed without the row and column corrections; corrected measurements were normalized by the median of each plate (median calculated using only colonies between the 40th and 80th percentiles due to the high number of strains with impaired fitness). For each condition, the measurements were then normalized by the median of that condition (median of the data between the 40th and 80th percentiles) and summarized by the mean and standard deviation for each strain. A similar procedure was used to determine the colony sizes in the AID-v1 library grown according to Fig. 2c.

To identify strains with impaired growth upon degradation of the AID-tagged protein, normalized colony sizes of *OsTIR1*$^+$ or *OsTIR1*$^-$ strains in the AID-v1 library or normalized colony sizes of AID-v2 strains on control and 5-Ph-IAA plates were compared with a two-sided t-test and p-values were adjusted for multiple testing using the Benjamini-Hochberg method. Strains with impaired fitness were defined as follows:

- AID-v1 library: size(*OsTIR1*$^+$)/size(*OsTIR1*$^-$) < 0.8 and p-value < 0.05 (Fig. 3a);

- AID-v2 library: size(5-Ph-IAA)/size(control) < 0.8 and p-value < 0.05 (Fig. S4a).

Chemical-genetic interaction (CGI) scores were calculated for each ORF using the normalized median-centered colony sizes and the multiplicative model (Baryshnikova et al., 2010b) as follows:

CGI score = size(5-Ph-IAA, GA) – size(5-Ph-IAA) x size(GA).

Finally, colony sizes in the double perturbation condition (5-Ph-IAA, GA) were compared against the product of sizes from the single perturbation (5-Ph-IAA and GA) with a two-sided t-test and p-values were adjusted for multiple testing using the Benjamini-Hochberg method. Significant negative chemical-genetic interactions were defined as follows: size(5-Ph-IAA, GA) ≤ 0.9, CGI score ≤ -0.2 and p-value < 0.05. The identified genes were mapped to gene ontology (GO) terms using the GO slim mapper in the Saccharomyces genome database with GO version 2024-01 (Wong et al., 2023) and grouped into broader functional categories (Fig. 4d, Fig. S5c) as follows:

- transcription GO terms: transcription by RNA polymerase I, transcription by RNA polymerase II, mRNA processing, rRNA processing and RNA catabolic process;
- chromatin organization GO terms: chromatin organization;
- DNA damage response GO terms: DNA repair, DNA recombination and DNA damage response;
- cell cycle GO terms: meiotic cell cycle, mitotic cell cycle, regulation of cell cycle, DNA replication, sporulation and chromosome segregation;
- metabolism GO terms: amino acid metabolic process, vitamin metabolic process, generation of precursor metabolites and energy, carbohydrate metabolic process and nucleobase-containing small molecule metabolic process;
- proteostasis GO terms: protein glycosylation, protein folding, protein modification by small protein conjugation or removal, and proteolysis involved in protein catabolic process;
- intracellular trafficking and lipid metabolism GO terms: endosomal transport, transmembrane transport, vacuole organization, endocytosis, Golgi vesicle transport, membrane fusion, vesicle organization, lipid metabolic process and protein targeting.

Acknowledgements

We thank Helle Ulrich for reagents. We thank the IMB Flow Cytometry Core Facility for the use of their instruments. Funding of the German Research Foundation supported the BD LSRFortessa SORP (P#210253511). The IMB Media Lab and the IMB Protein Production facility are gratefully acknowledged for support with growth media and reagents. This work was supported by the European Research Council (ERC-2017-STG#759427 to A.K.).

Author Contributions Statement

Conceptualization: BL, AK; experimental investigation: EG, KAJN; data analysis: EG, KJ, JJF, SS; writing-original draft: AK; writing-review and editing: AK, BL, EG, KAJN; supervision: BL, AK.; funding acquisition: BL, AK.

Competing Interests Statement

The authors declare no competing interests.

References

Baryshnikova A, Costanzo M, Dixon S, Vizeacoumar FJ, Myers CL, Andrews B, Boone C. 2010a. Synthetic genetic array (SGA) analysis in Saccharomyces cerevisiae and Schizosaccharomyces pombe. *Methods Enzymol* **470**:145–179. doi:10.1016/S0076-6879(10)70007-0

Baryshnikova A, Costanzo M, Kim Y, Ding H, Koh J, Toufighi K, Youn J-YY, Ou J, San Luis B-JJ, Bandyopadhyay S, Hibbs M, Hess D, Gingras A-CC, Bader GD, Troyanskaya OG, Brown GW, Andrews B, Boone C, Myers CL. 2010b. Quantitative analysis of fitness and genetic interactions in yeast on a genome scale. *Nat Methods* **7**:1017–1024. doi:10.1038/nmeth.1534

Bateman A, Martin MJ, Orchard S, Magrane M, Ahmad S, Alpi E, Bowler-Barnett EH, Britto R, Bye-A-Jee H, Cukura A, Denny P, Dogan T, Ebenezer TG, Fan J, Garmiri P, da Costa Gonzales LJ, Hatton-Ellis E, Hussein A, Ignatchenko A, Insana G, Ishtiaq R, Joshi V, Jyothi D, Kandasaamy S, Lock A, Luciani A, Lugaric M, Luo J, Lussi Y, MacDougall A, Madeira F, Mahmoudy M, Mishra A, Moulang K, Nightingale A, Pundir S, Qi G, Raj S, Raposo P, Rice DL, Saidi R, Santos R, Speretta E, Stephenson J, Totoo P, Turner E, Tyagi N, Vasudev P, Warner K, Watkins X, Zaru R, Zellner H, Bridge AJ, Aimo L, Argoud-Puy G, Auchincloss AH, Axelsen KB, Bansal P, Baratin D, Batista Neto TM, Blatter MC, Bolleman JT, Boutet E, Breuza L, Gil BC, Casals-Casas C, Echioukh KC, Coudert E, Cuche B, de Castro E, Estreicher A, Famiglietti ML, Feuermann M, Gasteiger E, Gaudet P, Gehant S, Gerritsen V, Gos A, Gruaz N, Hulo C, Hyka-Nouspikel N, Jungo F, Kerhornou A, Le Mercier P, Lieberherr D, Masson P, Morgat A, Muthukrishnan V, Paesano S, Pedruzzi I, Pilbout S, Pourcel L, Poux S, Pozzato M, Pruess M, Redaschi N, Rivoire C, Sigrist CJA, Sonesson K, Sundaram S, Wu CH, Arighi CN, Arminski L, Chen C, Chen Y, Huang H, Laiho K, McGarvey P, Natale DA, Ross K, Vinayaka CR, Wang Q, Wang Y, Zhang J. 2023. UniProt: the Universal Protein Knowledgebase in 2023. *Nucleic Acids Res* **51**:D523–D531. doi:10.1093/nar/gkac1052

Beilharz T, Egan B, Silver PA, Hofmann K, Lithgow T. 2003. Bipartite signals mediate subcellular targeting of tail-anchored membrane proteins in Saccharomyces cerevisiae. *Journal of Biological Chemistry* **278**:8219–8223. doi:10.1074/jbc.M212725200

Békés M, Langley DR, Crews CM. 2022. PROTAC targeted protein degraders: the past is prologue. *Nat Rev Drug Discov* **21**:181–200. doi:10.1038/s41573-021-00371-6

Ben-Aroya S, Coombes C, Kwok T, O'Donnell KA, Boeke JD, Hieter P. 2008. Toward a comprehensive temperature-sensitive mutant repository of the essential genes of Saccharomyces cerevisiae. *Mol Cell* **30**:248–258. doi:10.1016/j.molcel.2008.02.021

Bordonné R. 2000. Functional characterization of nuclear localization signals in yeast Sm proteins. *Mol Cell Biol* **20**:7943–7954. doi:10.1128/MCB.20.21.7943-7954.2000

Botstein D, Fink GR. 2011. Yeast: an experimental organism for 21st Century biology. *Genetics* **189**:695–704. doi:10.1534/genetics.111.130765

Breker M, Gymrek M, Schuldiner M. 2013. A novel single-cell screening platform reveals proteome plasticity during yeast stress responses. *Journal of Cell Biology* **200**:839–850. doi:10.1083/jcb.201301120

Breslow DK, Cameron DM, Collins SR, Schuldiner M, Stewart-Ornstein J, Newman HW, Braun S, Madhani HD, Krogan NJ, Weissman JS. 2008. A comprehensive strategy enabling high-resolution functional analysis of the yeast genome. *Nat Methods* **5**:711–718. doi:10.1038/nmeth.1234

Burri L, Lithgow T. 2004. A complete set of SNAREs in yeast. *Traffic* **5**:45–52. doi:10.1046/J.1600-0854.2003.00151.X

Chang M, Bellaoui M, Boone C, Brown GW. 2002. A genome-wide screen for methyl methanesulfonate-sensitive mutants reveals genes required for S phase progression in the presence of DNA damage. *Proceedings of the National Academy of Sciences* **99**:16934–16939. doi:10.1073/pnas.262669299

De Groot PWJ, Hellingwerf KJ, Klis FM. 2003. Genome-wide identification of fungal GPI proteins. *Yeast* **20**:781–796. doi:10.1002/yea.1007

Després PC, Dubé AK, Seki M, Yachie N, Landry CR. 2020. Perturbing proteomes at single residue resolution using base editing. *Nat Commun* **11**:1–13. doi:10.1038/s41467-020-15796-7

Fung JJ, Blöcher-Juárez K, Khmelinskii A. 2022. High-throughput analysis of protein turnover with tandem fluorescent protein timers. *Methods in Molecular Biology* **2378**:85–100. doi:10.1007/978-1-0716-1732-8_6

Game JC, Mortimer RK. 1974. A genetic study of x-ray sensitive mutants in yeast. *Mutat Res* **24**:281–292. doi:10.1016/0027-5107(74)90176-6

Giaever G, Chu AM, Ni L, Connelly C, Riles L, Véronneau S, Dow S, Lucau-Danila A, Anderson K, André B, Arkin AP, Astromoff A, El Bakkoury M, Bangham R, Benito R, Brachat S, Campanaro S, Curtiss M, Davis K, Deutschbauer A, Entian KD, Flaherty P, Foury F, Garfinkel DJ, Gerstein M, Gotte D, Güldener U, Hegemann JH, Hempel S, Herman Z, Jaramillo DF, Kelly DE, Kelly SL, Kötter P, LaBonte D, Lamb DC, Lan N, Liang H, Liao H, Liu L, Luo C, Lussier M, Mao R, Menard P, Ooi SL, Revuelta JL, Roberts CJ, Rose M, Ross-Macdonald P, Scherens B, Schimmack G, Shafer B, Shoemaker DD, Sookhai-Mahadeo S, Storms RK, Strathern JN, Valle G, Voet M, Volckaert G, Wang CY, Ward TR, Wilhelmy J, Winzeler EA, Yang Y, Yen G, Youngman E, Yu K, Bussey H, Boeke JD, Snyder M, Philippsen P, Davis RW, Johnston M. 2002. Functional profiling of the Saccharomyces cerevisiae genome. *Nature* **418**:387–391. doi:10.1038/nature00935

Giaever G, Nislow C. 2014. The yeast deletion collection: a decade of functional genomics. *Genetics* **197**:451–465. doi:10.1534/genetics.114.161620

Giolito ML, Bigliani G, Meinero R, Taubas JV. 2024. Palmitoylation of CYSTM (CYSPD) proteins in yeast. *Journal of Biological Chemistry* **300**:105609. doi:10.1016/j.jbc.2023.105609

Gíslason MH, Nielsen H, Almagro Armenteros JJ, Johansen AR. 2021. Prediction of GPI-anchored proteins with pointer neural networks. *Curr Res Biotechnol* **3**:6–13. doi:10.1016/j.crbiot.2021.01.001

Hahn S, Maurer P, Caesar S, Schlenstedt G. 2008. Classical NLS proteins from Saccharomyces cerevisiae. *J Mol Biol* **379**:678–694. doi:10.1016/j.jmb.2008.04.038

Huang ME, Facca C, Fatmi Z, Baïlle D, Bénakli S, Vernis L. 2016. DNA replication inhibitor hydroxyurea alters Fe-S centers by producing reactive oxygen species in vivo. *Sci Rep* **6**. doi:10.1038/srep29361

Huh W-K, Falvo J V, Gerke LC, Carroll AS, Howson RW, Weissman JS, O'Shea EK. 2003. Global analysis of protein localization in budding yeast. *Nature* **425**:686–691. doi:10.1038/nature02026

Janke C, Magiera MM, Rathfelder N, Taxis C, Reber S, Maekawa H, Moreno-Borchart A, Doenges G, Schwob E, Schiebel E, Knop M. 2004. A versatile toolbox for PCR-based tagging of yeast genes: new fluorescent proteins, more markers and promoter substitution cassettes. *Yeast* **21**:947–962. doi:10.1002/yea.1142

Kanemaki M, Sanchez-Diaz A, Gambus A, Labib K. 2003. Functional proteomic identification of DNA replication proteins by induced proteolysis in vivo. *Nature* **423**:720–724. doi:10.1038/nature01692

Kim H, Melén K, Osterberg M, von Heijne G. 2006. A global topology map of the Saccharomyces cerevisiae membrane proteome. *Proc Natl Acad Sci U S A* **103**:11142–11147. doi:10.1073/pnas.0604075103

Knop M, Siegers K, Pereira G, Zachariae W, Winsor B, Nasmyth K, Schiebel E. 1999. Epitope tagging of yeast genes using a PCR-based strategy: more tags and improved practical routines. *Yeast* **15**:963–972. doi:10.1002/(SICI)1097-0061(199907)15:10B<963::AID-YEA399>3.0.CO;2-W

Kuong KJ, Kuzminov A. 2009. Cyanide, peroxide and nitric oxide formation in solutions of hydroxyurea causes cellular toxicity and may contribute to its therapeutic potency. *J Mol Biol* **390**:845–862. doi:10.1016/j.jmb.2009.05.038

Lee RS, Geronimo CL, Liu L, Twarowski JM, Malkova A, Zakian VA. 2023. Identification of the nuclear localization signal in the Saccharomyces cerevisiae Pif1 DNA helicase. *PLoS Genet* **19**:e1010853. doi:10.1371/journal.pgen.1010853

Lewis MJ, Pelham HRB. 2002. A new yeast endosomal SNARE related to mammalian syntaxin 8. *Traffic* **3**:922–929. doi:10.1034/J.1600-0854.2002.31207.X

Li F, Jiang T, Li Q, Ling X. 2017. Camptothecin (CPT) and its derivatives are known to target topoisomerase I (Top1) as their mechanism of action: did we miss something in CPT analogue molecular targets for treating human disease such as cancer? *Am J Cancer Res* **7**:2350.

Li Z, Vizeacoumar FJ, Bahr S, Li J, Warringer J, Vizeacoumar FS, Min R, VanderSluis B, Bellay J, Devit M, Fleming JA, Stephens A, Haase J, Lin Z-Y, Baryshnikova A, Lu H, Yan Z, Jin K, Barker S, Datti A, Giaever G, Nislow C, Bulawa C, Myers CL, Costanzo M, Gingras A-C, Zhang Z, Blomberg A, Bloom K, Andrews B, Boone C. 2011. Systematic exploration of essential yeast gene function with temperature-sensitive mutants. *Nat Biotechnol* **29**:361–367. doi:10.1038/nbt.1832

Meurer M, Duan Y, Sass E, Kats I, Herbst K, Buchmuller BC, Dederer V, Huber F, Kirrmaier D, Štefl M, Van Laer K, Dick TP, Lemberg MK, Khmelinskii A, Levy ED, Knop M. 2018. Genome-wide C-SWAT library for high-throughput yeast genome tagging. *Nat Methods* **15**:598–600. doi:10.1038/s41592-018-0045-8

Mnaimneh S, Davierwala AP, Haynes J, Moffat J, Peng WT, Zhang W, Yang X, Pootoolal J, Chua G, Lopez A, Trochesset M, Morse D, Krogan NJ, Hiley SL, Li Z, Morris Q, Grigull J, Mitsakakis N, Roberts CJ, Greenblatt JF, Boone C, Kaiser CA, Andrews BJ, Hughes TR. 2004. Exploration of essential gene functions via titratable promoter alleles. *Cell* **118**:31–44. doi:10.1016/j.cell.2004.06.013

Morawska M, Ulrich HD. 2013. An expanded tool kit for the auxin-inducible degron system in budding yeast. *Yeast* **30**:341–351. doi:10.1002/yea.2967

Musiałek MW, Rybaczek D. 2021. Hydroxyurea - the good, the bad and the ugly. *Genes (Basel)* **12**. doi:10.3390/genes12071096

Nishimura K, Fukagawa T, Takisawa H, Kakimoto T, Kanemaki M. 2009. An auxin-based degron system for the rapid depletion of proteins in nonplant cells. *Nat Methods* **6**:917–922. doi:10.1038/nmeth.1401

Nötzel C, Lingner T, Klingenberg H, Thoms S. 2016. Identification of new fungal peroxisomal matrix proteins and revision of the PTS1 consensus. *Traffic* **17**:1110–1124. doi:10.1111/tra.12426

Parsons AB, Brost RL, Ding H, Li Z, Zhang C, Sheikh B, Brown GW, Kane PM, Hughes TR, Boone C. 2003. Integration of chemical-genetic and genetic interaction data links bioactive compounds to cellular target pathways. *Nat Biotechnol* **22**:62–69. doi:10.1038/nbt919

R Core Team. 2020. R: A language and environment for statistical computing. https://www.r-project.org/

Resnick Michael A. 1969. Genetic control of radiation sensitivity in Saccharomyces cerevisiae. *Genetics* **62**:519–531. doi:10.1093/genetics/62.3.519

Schuldiner M, Metz J, Schmid V, Denic V, Rakwalska M, Schmitt HD, Schwappach B, Weissman JS. 2008. The GET complex mediates insertion of tail-anchored proteins into the ER membrane. *Cell* **134**:634–645. doi:10.1016/j.cell.2008.06.025

Sherwood PW, Carlson M. 1999. Efficient export of the glucose transporter Hxt1p from the endoplasmic reticulum requires Gsf2p. *Proc Natl Acad Sci U S A* **96**:7415–7420. doi:10.1073/pnas.96.13.7415

Simočková M, Holič R, Tahotná D, Patton-Vogt J, Griač P. 2008. Yeast Pgc1p (YPL206c) controls the amount of phosphatidylglycerol via a phospholipase C-type degradation mechanism. *Journal of Biological Chemistry* **283**:17107–17115. doi:10.1074/jbc.M800868200

Singh A, Xu Y-J. 2016. The cell killing mechanisms of hydroxyurea. *Genes (Basel)* **7**:99. doi:10.3390/genes7110099

Snyder NA, Kim A, Kester L, Gale AN, Studer C, Hoepfner D, Roggo S, Helliwell SB, Cunningham KW. 2019. Auxin-inducible depletion of the essentialome suggests inhibition of TORC1 by auxins and inhibition of Vrg4 by SDZ 90-215, a natural antifungal cyclopeptide. *G3* **9**:829–840. doi:10.1534/g3.118.200748

Somashekara SC, Muniyappa K. 2022. Dual targeting of *Saccharomyces cerevisiae* Pso2 to mitochondria and the nucleus, and its functional relevance in the repair of DNA interstrand crosslinks. *G3* **12**. doi:10.1093/g3journal/jkac066

Symington LS. 2002. Role of *RAD52* epistasis group genes in homologous recombination and double-strand break repair. *Microbiology and Molecular Biology Reviews* **66**:630–670. doi:10.1128/MMBR.66.4.630-670.2002

Takano Y, Nakatsukasa K. 2023. Hydroxyurea inhibits ERAD-L independently of S-phase arrest in budding yeast. *bioRxiv*. doi:10.1101/2023.01.22.525111

Tong AH, Evangelista M, Parsons AB, Xu H, Bader GD, Pagé N, Robinson M, Raghibizadeh S, Hogue CW, Bussey H, Andrews B, Tyers M, Boone C. 2001. Systematic genetic analysis with ordered arrays of yeast deletion mutants. *Science* **294**:2364–2368. doi:10.1126/science.1065810

Van Leeuwen J, Pons C, Mellor JC, Yamaguchi TN, Friesen H, Koschwanez J, Ušaj MM, Pechlaner M, Takar M, Ušaj M, Vander Sluis B, Andrusiak K, Bansal P, Baryshnikova A, Boone CE, Cao J, Cote A, Gebbia M, Horecka G, Horecka I, Kuzmin E, Legro N, Liang W, Van Lieshout N, McNee M, San Luis BJ, Shaeri F, Shuteriqi E, Sun S, Yang L, Youn JY, Yuen M, Costanzo M, Gingras AC, Aloy P, Oostenbrink C, Murray A, Graham TR, Myers CL, Andrews BJ, Roth FP, Boone C. 2016. Exploring genetic suppression interactions on a global scale. *Science* **354**. doi:10.1126/science.aag0839

Venancio TM, Aravind L. 2010. CYSTM, a novel cysteine-rich transmembrane module with a role in stress tolerance across eukaryotes. *Bioinformatics* **26**:149–152. doi:10.1093/bioinformatics/btp647

Wagih O, Parts L. 2014. Gitter: A robust and accurate method for quantification of colony sizes from plate images. *G3: Genes, Genomes, Genetics* **4**:547–552. doi:10.1534/g3.113.009431

Wagih O, Usaj M, Baryshnikova A, VanderSluis B, Kuzmin E, Costanzo M, Myers CL, Andrews BJ, Boone CM, Parts L. 2013. SGAtools: One-stop analysis and visualization of array-based genetic interaction screens. *Nucleic Acids Res* **41**:W591-6. doi:10.1093/nar/gkt400

Weill U, Krieger G, Avihou Z, Milo R, Schuldiner M, Davidi D. 2019. Assessment of GFP tag position on protein localization and growth fitness in yeast. *J Mol Biol* **431**:636–641. doi:10.1016/J.JMB.2018.12.004

Weill U, Yofe I, Sass E, Stynen B, Davidi D, Natarajan J, Ben-Menachem R, Avihou Z, Goldman O, Harpaz N, Chuartzman S, Kniazev K, Knoblach B, Laborenz J, Boos F, Kowarzyk J, Ben-Dor S, Zalckvar E, Herrmann JM, Rachubinski RA, Pines O, Rapaport D, Michnick SW, Levy ED, Schuldiner M. 2018. Genome-wide SWAp-Tag yeast libraries for proteome exploration. *Nat Methods* **15**:617–622. doi:10.1038/s41592-018-0044-9

Winzeler EA, Shoemaker DD, Astromoff A, Liang H, Anderson K, Andre B, Bangham R, Benito R, Boeke JD, Bussey H, Chu AM, Connelly C, Davis K, Dietrich F, Dow SW, El Bakkoury M, Foury F, Friend SH, Gentalen E, Giaever G, Hegemann JH, Jones T, Laub M, Liao H, Liebundguth N, Lockhart DJ, Lucau-Danila A, Lussier M, M'Rabet N, Menard P, Mittmann M, Pai C, Rebischung C, Revuelta JL, Riles L, Roberts CJ, Ross-MacDonald P, Scherens B, Snyder M, Sookhai-Mahadeo S, Storms RK, Véronneau S, Voet M, Volckaert G, Ward TR, Wysocki R, Yen GS, Yu K, Zimmermann K, Philippsen P, Johnston M, Davis RW. 1999. Functional characterization of the S. cerevisiae genome by gene deletion and parallel analysis. *Science* **285**:901–906.

Wong ED, Miyasato SR, Aleksander S, Karra K, Nash RS, Skrzypek MS, Weng S, Engel SR, Cherry JM. 2023. Saccharomyces genome database update: server architecture, pan-genome nomenclature, and external resources. *Genetics* **224**. doi:10.1093/genetics/iyac191

Wyatt MD, Pittman DL. 2006. Methylating agents and DNA repair responses: methylated bases and sources of strand breaks. *Chem Res Toxicol* **19**:1580–1594. doi:10.1021/tx060164e

Yesbolatova A, Saito Y, Kitamoto N, Makino-Itou H, Ajima R, Nakano R, Nakaoka H, Fukui K, Gamo K, Tominari Y, Takeuchi H, Saga Y, Hayashi K, Kanemaki MT. 2020. The auxin-inducible degron 2 technology provides sharp degradation control in yeast, mammalian cells, and mice. *Nat Commun* **11**:5701. doi:10.1038/s41467-020-19532-z

Yofe I, Weill U, Meurer M, Chuartzman S, Zalckvar E, Goldman O, Ben-Dor S, Schütze C, Wiedemann N, Knop M, Khmelinskii A, Schuldiner M. 2016. One library to make them all: Streamlining the creation of yeast libraries via a SWAp-Tag strategy. *Nat Methods* **13**:371–378. doi:10.1038/nmeth.3795

Zvonarev A, Ledova L, Ryazanova L, Valiakhmetov A, Farofonova V, Kulakovskaya T. 2023. The YBR056W-A and its ortholog YDR034W-B of S. cerevisiae belonging to CYSTM family participate in manganese stress overcoming. *Genes (Basel)* **14**:987. doi:10.3390/genes14050987

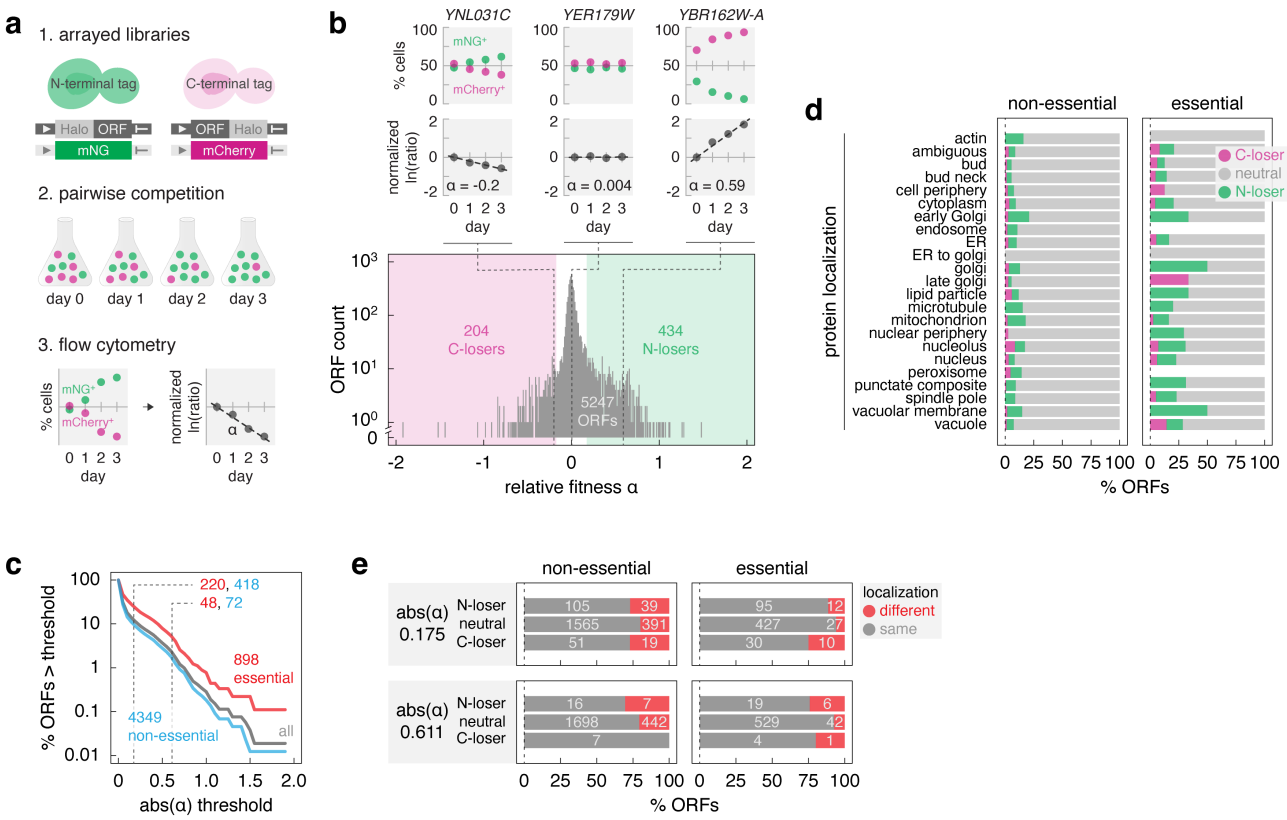

Figure 1. Fitness impact of N- vs C-terminal protein tagging.

a – Competition assay to compare fitness of strains with N- or C-terminally tagged proteins. Pairs of strains with the same open reading frame (ORF) tagged at the endogenous chromosomal locus are co-cultured. The percentage of each cell type in the population is followed with flow cytometry using strain-specific fluorescent markers expressed from the constitutive *GPD* promoter (mNeonGreen (mNG), green or mCherry, magenta). The slope α of a linear fit to ln(mCherry+ cells/mNG+ cells) over time represents the relative fitness of the two strains (α > 0, competitive advantage of the *ORF-Halo* strain).

b – Genome-wide assessment of N- vs C-terminal protein tagging impact on fitness. Distribution of relative fitness for 5247 ORFs assayed according to **a**. ORFs with α < -0.076 are defined as C-losers (C-terminal tagging impairs fitness, magenta area), α > 0.076 – N-losers (green area). Top, percentage of mCherry+ and mNG+ cells and linear fit to the log(mCherry+/mNG+ cells) over time for three representative ORFs.

c – Percentage of ORFs differentially affected by N- vs C-terminal tagging as a function of a relative fitness threshold. Number of ORFs, essential (red) or non-essential (blue), differentially affected at two thresholds (dashed lines, abs(α) = 0.175 (5% fitness difference) and 0.611 (20%), Methods) is indicated.

d – Frequency of relative fitness differences according to protein localization. Subcellular localization based on fluorescence microscopy imaging of 3827 strains expressing C-terminally GFP-tagged proteins (Huh et al., 2003).

e – Proteins with differential localization of N- and C-terminally GFP tagged variants (Huh et al., 2003; Weill et al., 2018), stratified by gene essentiality and differential fitness according to **b**. N-loser, neutral and C-loser ORFs defined at two differential fitness thresholds. Number of ORFs in each group is indicated.

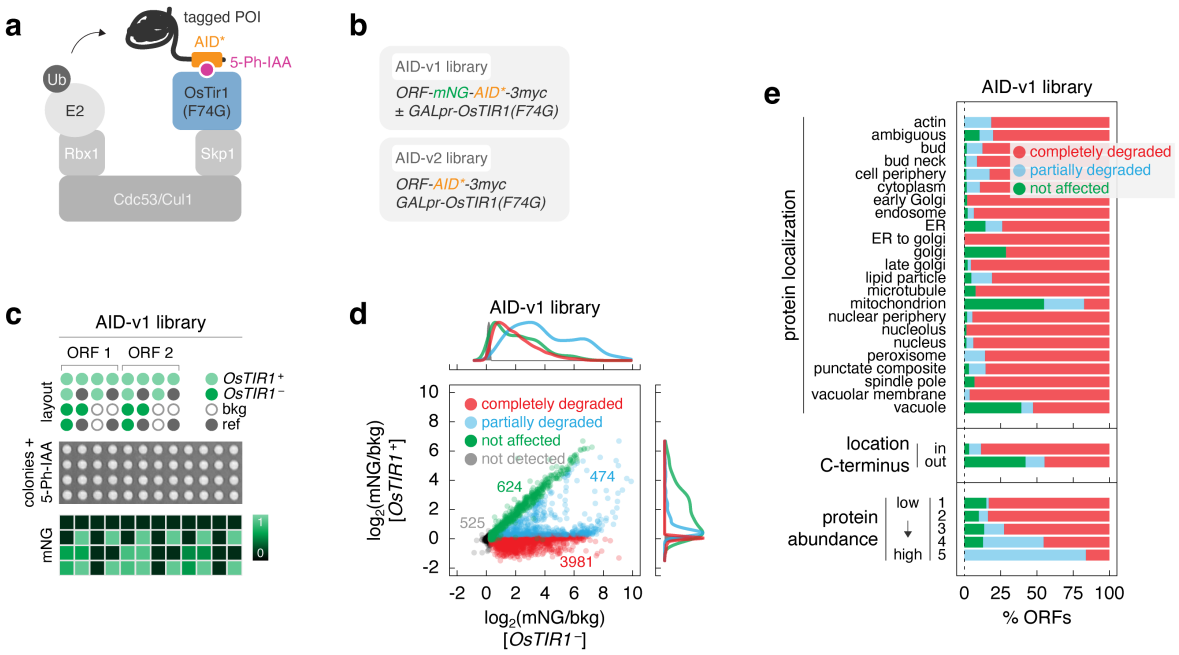

Figure 2. Efficient protein degradation with genome-wide AID libraries.

a – Features of the auxin-inducible degron system in the AID libraries. Proteins with a C-terminal AID* tag can be ubiquitinated and degraded in the presence of 5-Ph-IAA upon expression of the F-box protein OsTir1.
b – Different tags used in the AID libraries. Expression of *OsTIR1* is controlled by the galactose-inducible *GAL* promoter.
c – Characterization of the AID-v1 library with fluorescence measurements of colony arrays. Top, for each ORF, mNG-AID*-3myc-tagged strains with (+) or without (-) the *GALpr-OsTIR1* construct were placed next to each other. A reference strain (ref, with an abundant mNG-tagged protein, for correction of spatial and plate effects) and a strain without a fluorescent tag (bkg, for background correction) were included in each 4x4 group. Middle, colony arrays were grown on galactose medium with 1 µM 5-Ph-IAA. Bottom, example heatmap of mNG fluorescence intensities.
d – Protein levels (mNG signal in units of background fluorescence, mNG/bkg) in the AID-v1 library determined according to **c**. Not detected, strains without a detectable mNG signal in the absence of *OsTIR1* (mNG/bkg(*OsTIR1*⁻) ≤ 1.2). Detectable proteins were classified by the extent of *OsTIR1*-dependent degradation (Methods). Top and right, normalized frequency distributions of protein levels in each category.
e – Frequency of *OsTIR1*-dependent degradation phenotypes in the AID-v1 library according to protein localization, location of the C-terminus (cytosol – in, lumen of organelles or extracellular – out) for membrane proteins according to (Kim et al., 2006) or abundance of the mNG-AID*-3myc-tagged proteins.

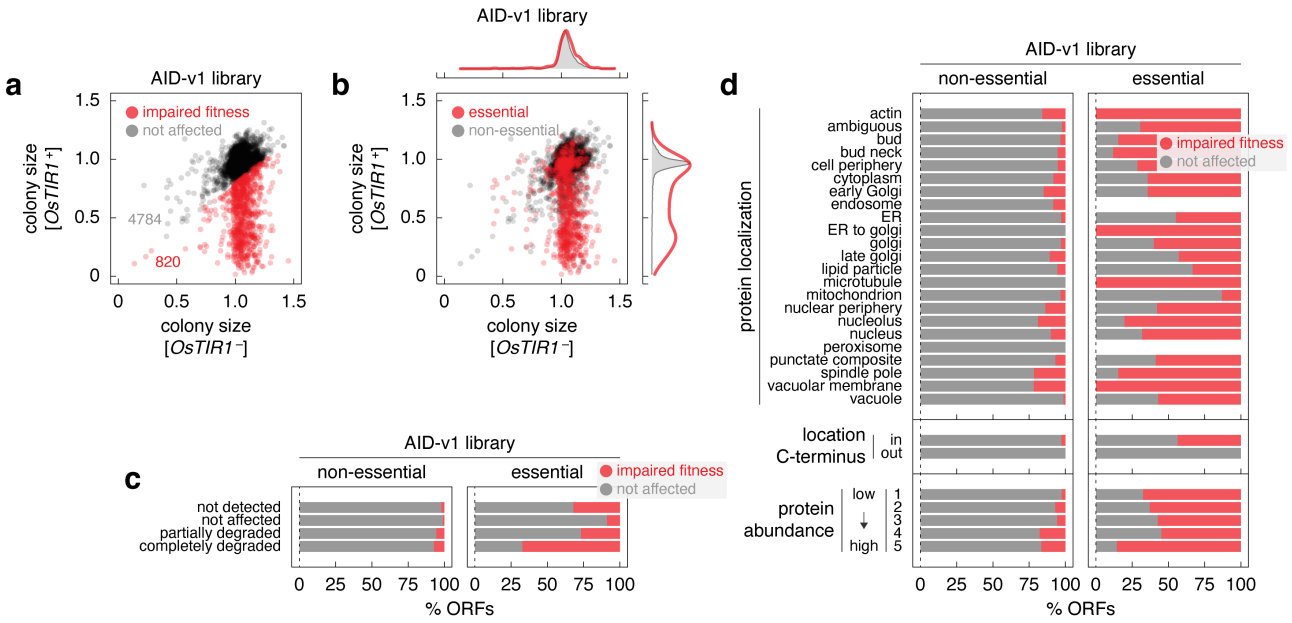

Figure 3. Fitness defects in the AID libraries upon induction of protein degradation.

a, b – Normalized colony sizes in the AID-v1 library grown according to Fig. 2c. **b**, essential and non-essential ORFs are marked; top and right, normalized frequency distributions of normalized colony sizes in each category.

c, d – Frequency of *OsTIR1*-dependent fitness defects in the AID-v1 library according to the extent of *OsTIR1*-dependent degradation phenotypes (**c**) or according to localization, location of the C-terminus (cytosol – in, lumen of organelles or extracellular – out) or abundance of the mNG-AID*-3myc-tagged proteins (**d**).

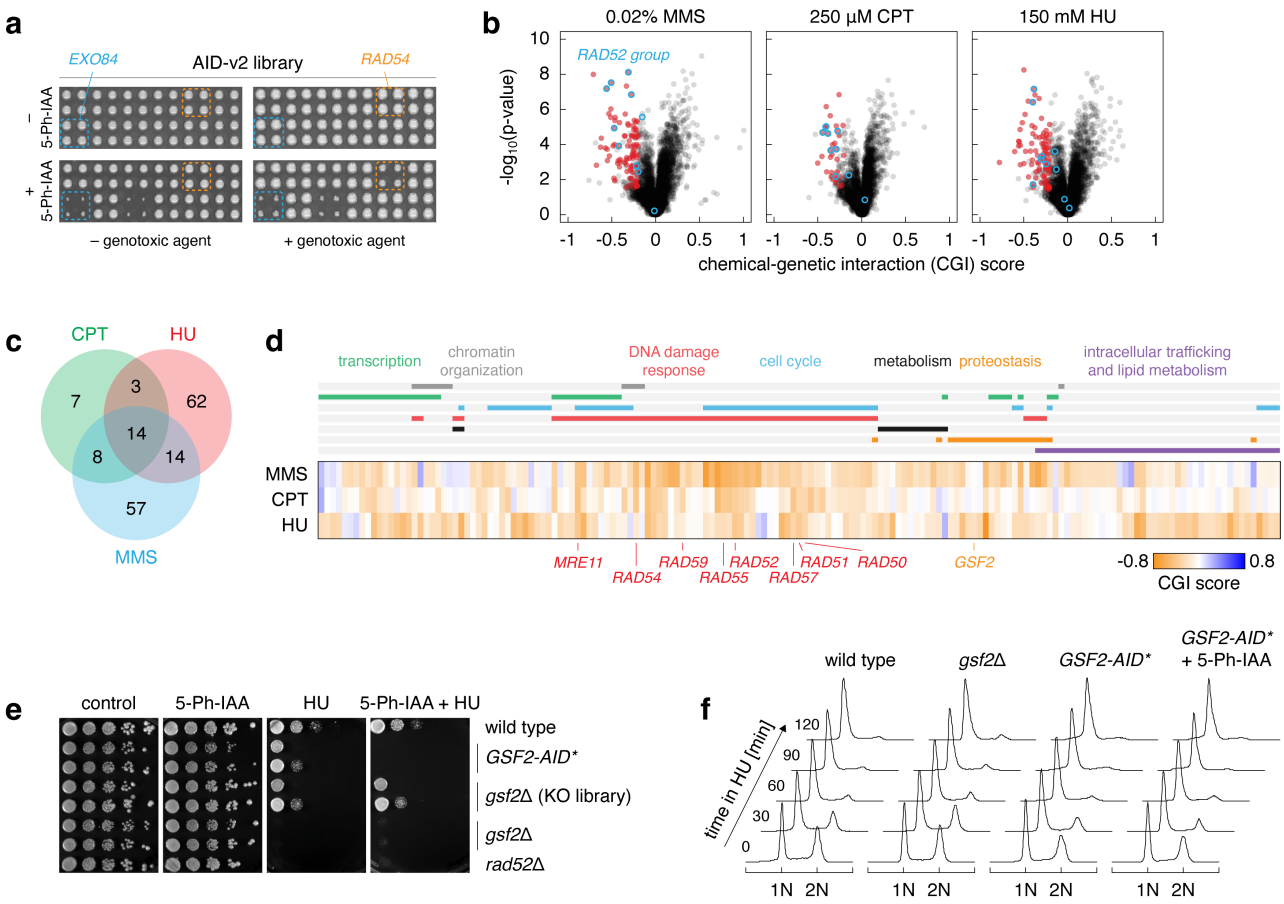

Figure 4. Genome-wide screens for DNA damage response factors.

a – Arrayed fitness screens. The AID-v2 library was grown on galactose media with or without MMS, CPT or HU as genotoxic agents (GAs).
b – Volcano plots of chemical-genetic interaction (CGI) scores between the AID alleles and the indicated GAs. Negative chemical-genetic interactors with each genotoxic agent (red, colony size (5-Ph-IAA + GA) ≤ 0.9, CGI score ≤ 0.2 and p-value < 0.05) and *RAD52* epistasis group genes (blue) are marked.
c, d – Venn diagram (**c**) and heatmap (**d**) of negative chemical-genetic interactors (red in **b**) with the three genotoxic agents. **d**, functional categories based on gene ontology terms (top, Methods) and *RAD52* epistasis group genes (bottom) are indicated.
e – Sensitivity of *GSF2* mutants to HU. Ten-fold serial dilutions of the indicated strains (GSF2-AID* strain from the AID-v2 library, *gsf2*Δ mutant from the haploid yeast knockout library and an independently constructed *gsf2*Δ strain) on galactose media with 5-Ph-IAA, HU or both compounds.
f – Flow cytometry analysis of DNA content in the presence of HU. Asynchronous cultures grown in galactose media (with or without 5-Ph-IAA) were treated with HU at time point zero. G1 and G2 peaks are labeled 1N and 2N, respectively.

Supplementary Figures

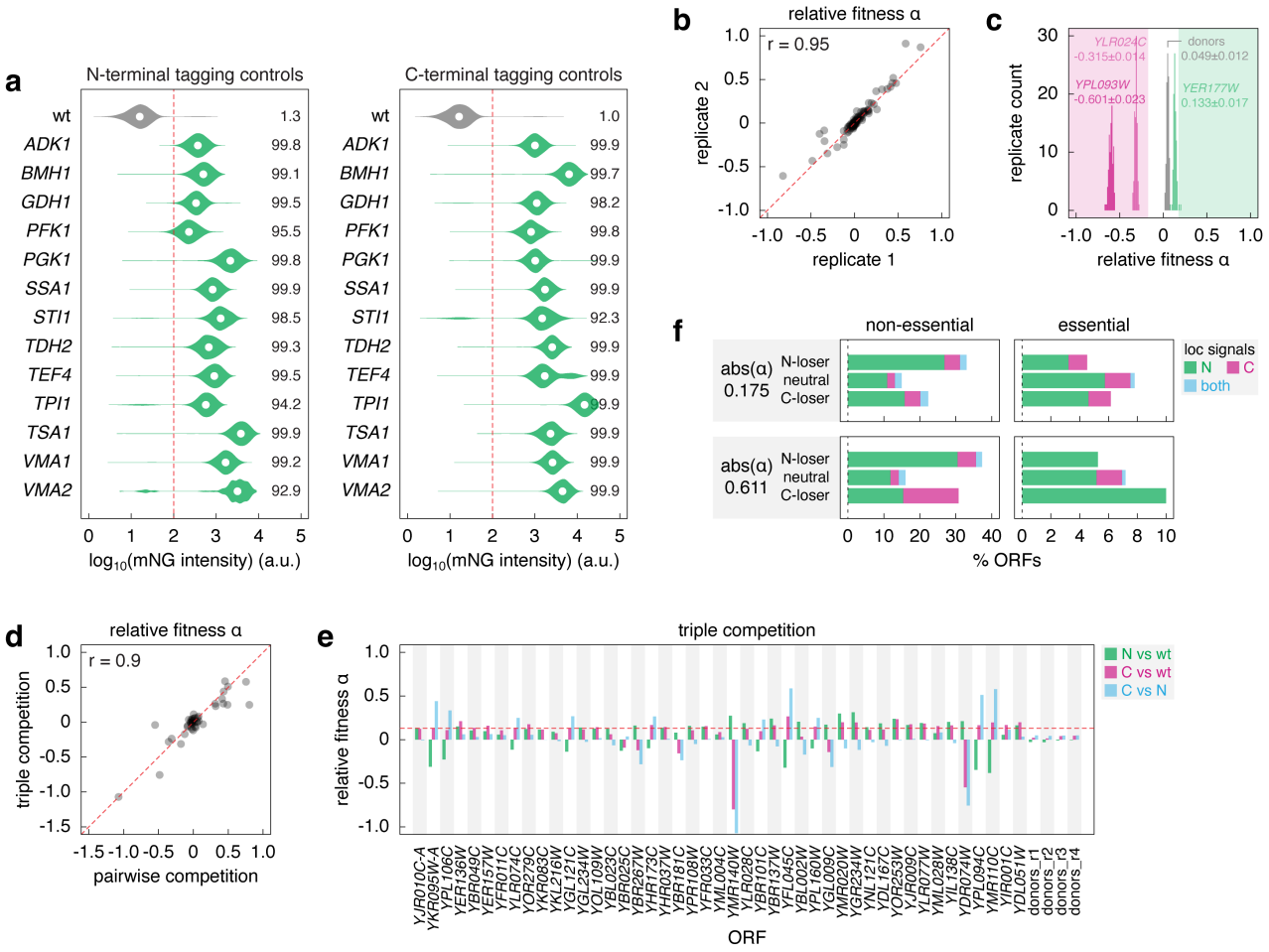

Figure S1. Fitness impact of N- vs C-terminal tagging.

a – Evaluation of the SWAT tagging efficiency during construction of the Halo-ORF and ORF-Halo libraries using donors with mNeonGreen (mNG) as the tag. Tagging was performed with 13 N-SWAT (left) or C-SWAT (right) strains for the indicated ORFs. Distributions of single-cell mNeonGreen fluorescence intensities measured with flow cytometry (10000 cells per strain). The percentage of cells with fluorescence above background (fluorescence of a wild type strain, red dashed line) is indicated.
b – Reproducibility of relative fitness estimation with the competition assay. Relative fitness of two replicates for 92 ORFs, determined as in Fig. 1a. r, pearson correlation coefficient.
c – Evaluation of technical noise in the competition assay. Distributions of relatives fitness determined as in Fig. 1a for the indicated ORFs and the pair of SWAT donor strains (no tagged ORF), 92 technical replicates per strain pair. Mean ± s.d. relative fitness is indicated.
d, e – Triple competition of 45 randomly selected pairs of Halo-ORF and ORF-Halo strains against a wild type strain lacking fluorescent markers. Relative fitness of Halo-tagged strains determined according to Fig. 1a and in the triple competition assay (**d**, Methods). Pairwise relative fitness of the three strains for each ORF in the triple competition assay (**e**, Methods). Median relative fitness (0.13) of N- and C-terminal variants against wild type (red dashed line, **e**).
f – Proteins with localization signals at the N-terminus, C-terminus or both protein termini, stratified by gene essentiality and differential fitness according to Fig. 1b. Analysis based on 997 validated or predicted localization signals: 611, 188 and 99 protein with signals at the N-terminus, the C-terminus or at both termini, respectively (Methods, Table S2). N-loser, neutral and C-loser ORFs defined at two differential fitness thresholds.

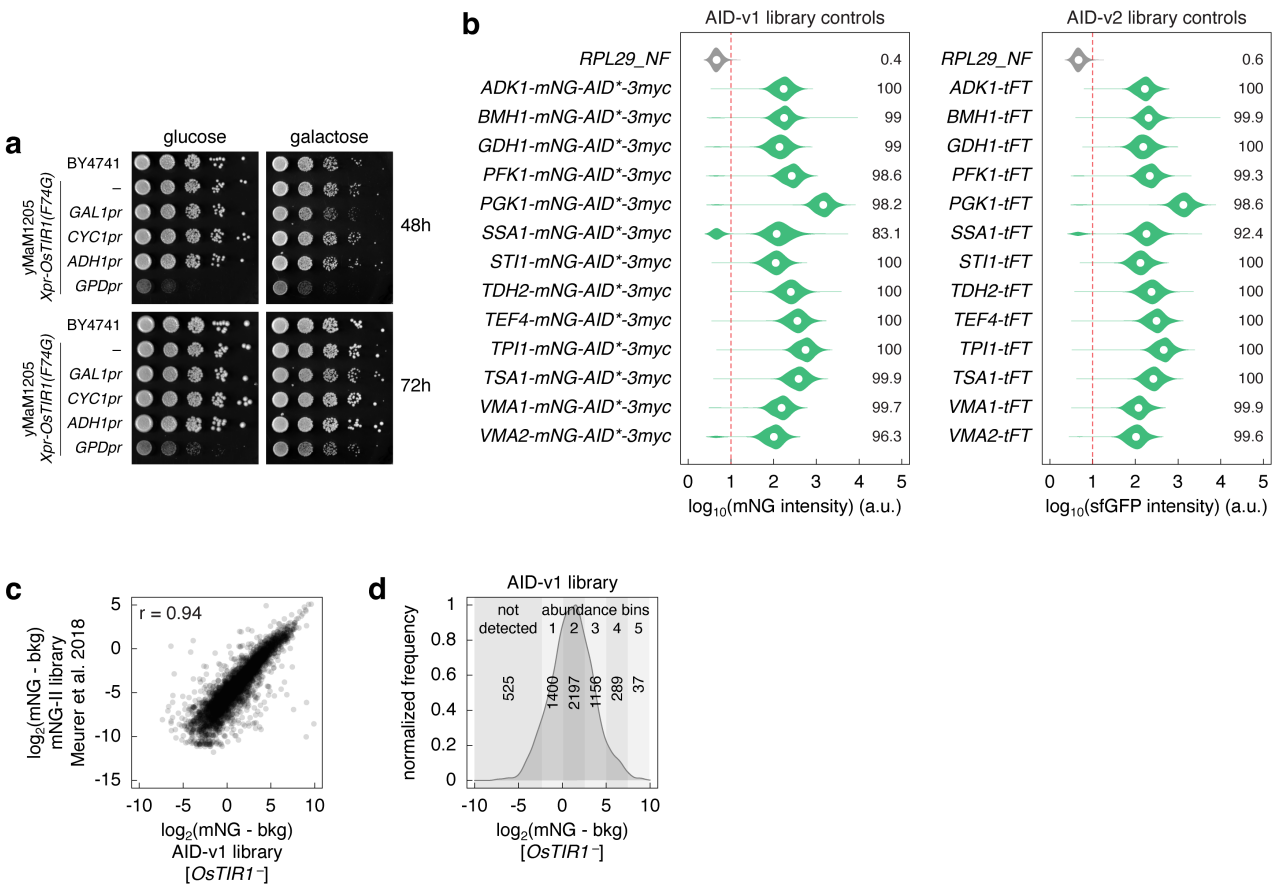

Figure S2. Construction and characterization of genome-wide AID libraries.

a – Fitness impact of *OsTIR1* expression from different promoters. Ten-fold serial dilutions of yeast strains on the indicated media with or without 1 µM 5-Ph-IAA.
b – Evaluation of the SWAT tagging efficiency during construction of the AID libraries. For the AID-v2 library, control tagging was performed with 13 C-SWAT strains for the indicated ORFs and a donor with the mCherry-sfGFP timer (tFT) as a tag. Distributions of single-cell mNeonGreen fluorescence intensities measured with flow cytometry (10000 cells per strain). The percentage of cells with fluorescence above background (fluorescence of a wild type strain, red dashed line) is indicated.
c – Comparison of relative protein expression levels measured with the AID-v1 library lacking *OsTIR1* and with the mNG-II library (ORF-mNG strains) (Meurer et al., 2018). Fluorescence intensities of colonies were corrected for background fluorescence.
d – Distribution of background-corrected mNG fluorescence intensities in the AID-v1 library, *OsTIR1*⁻ strains, determined according to Fig. 2c. Number of proteins in the not detected group (mNG/bkg(*OsTIR1*⁻) ≤ 1.2) and in five abundance bins used in Fig. 2e, 3d and Fig. S4d is indicated.

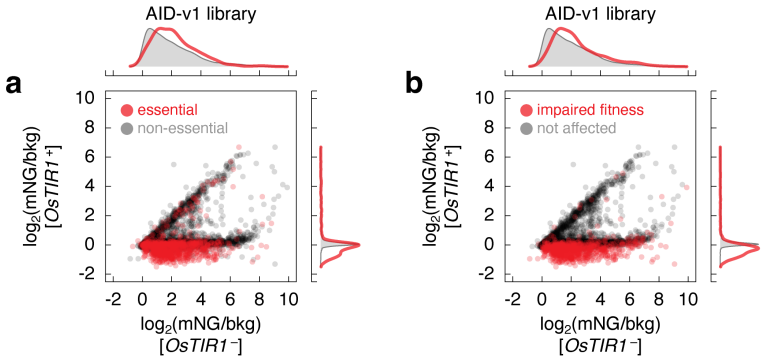

Figure S3. Characterization of the AID-v1 library.

a, b – Protein levels (mNG signal in units of background fluorescence, mNG/bkg) in the AID-v1 library determined according to Fig. 2c. Essential and non-essential ORFs (**a**) and strains with normal or impaired fitness based on colony size measurements (**b**) are marked. Top and right, normalized frequency distributions of protein levels in each category.

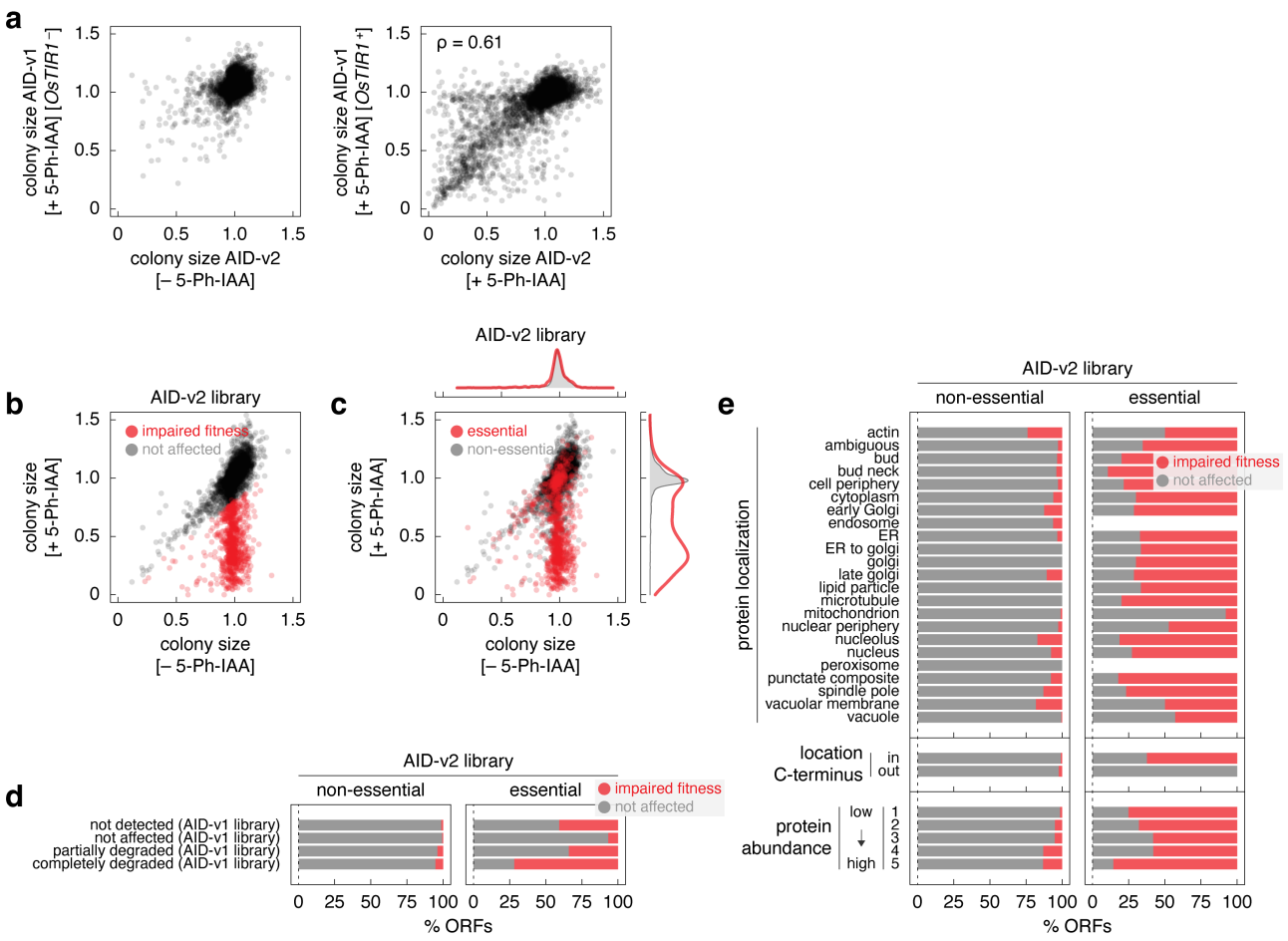

Figure S4. Characterization of the AID-v2 library.

a – Comparison of normalized colony sizes in the AID-v1 and AID-v2 libraries grown according to Fig. 2c and Fig. 4a, respectively. ρ, spearman correlation coefficient.
b, c – Normalized colony sizes in the AID-v2 library grown according to Fig. 4a on galactose medium with or without 1 µM 5-Ph-IAA. **c**, essential and non-essential ORFs are marked; top and right, normalized frequency distributions of normalized colony sizes in each category.
d, e – Frequency of 5-Ph-IAA-dependent fitness defects in the AID-v2 library according to the extent of *OsTIR1*-dependent degradation phenotypes in the AID-v1 library (**d**) or according to protein localization, location of the C-terminus (cytosol – in, lumen of organelles or extracellular – out) or protein abundance estimates from the AID1-v1 library (**e**).

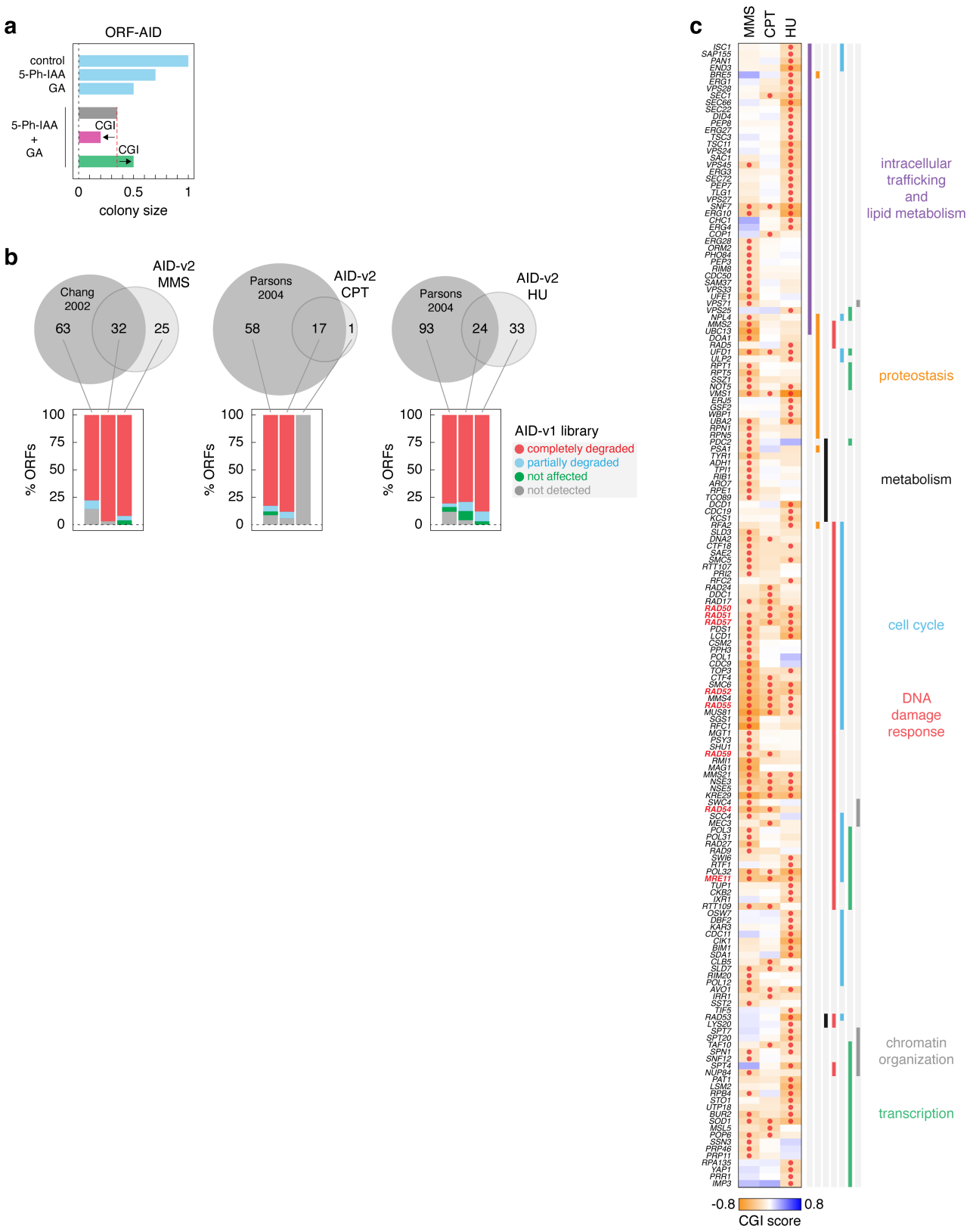

Figure S5. Genome-wide screens for DNA damage response factors.

a – Definition of chemical-genetic interaction (CGI). Fitness of an ORF-AID strain (normalized colony size, Methods) measured under four conditions: control (no perturbation), in the presence of 5-Ph-IAA (to induce degradation of the AID-tagged protein), GA (genotoxic agent) or both. Grey bar, expected fitness in the double perturbation condition (product of the fitness from the single perturbation conditions) in the absence of a CGI. Red and green bars, examples of negative and positive CGIs.

b – Top, overlap between chemical-genetic interactors identified with the AID-v2 library and previously identified resistance genes for MMS (Chang et al., 2002), CPT or HU (Parsons et al., 2003). Essential factors

identified with the AID-v2 library were excluded from the comparison. Bottom, frequency of *OsTIR1*-dependent degradation phenotypes in the AID-v1 library for the indicated sets of genes.
c – Heatmap of negative chemical-genetic interactors with MMS, CPT or HU, as in Fig. 4d. Gene names and significant interactors (red circles) with each genotoxic agent are indicated.

Supplementary Tables

Supplementary Table 1. Results of the genome-wide competition screen.

Supplementary Table 2. Terminal localization signals in the yeast proteome.

Supplementary Table 3. Characterization of the AID-v1 library.

Supplementary Table 4. Results of the genome-wide DDR screens.

Supplementary Table 5. Gene set enrichment analysis of resistance factors unique to each genotoxic agent.

Supplementary Table 6. Yeast strains.

Strain	Genotype	Source
BY4741	MATa his3Δ1 leu2Δ0 met15Δ0 ura3Δ0	
Y8205	MATalpha can1Δ::STE2pr-SpHIS5 lyp1Δ::STE3pr-LEU2 his3Δ1 leu2Δ0 ura3Δ0	
Y7092	MATalpha lyp1Δ his3Δ1 leu2Δ0 ura3Δ0 met15Δ0 can1Δ::STE2pr-SpHIS5	
yMaM1205	MATalpha lyp1Δ his3Δ1 leu2Δ0 ura3Δ0 met15Δ0 can1Δ::STE3pr-LEU2-GAL1pr-NLS-I-SCEI	
yKBJ0147	yMaM1205 leu2Δ::natNT2-TEF1pr-mCherry-CYC1term	this study
yKBJ0148	yMaM1205 leu2Δ::natNT2-TEF1pr-mNeonGreen-CYC1term	this study
yKBJ0200	yMaM1205 leu2Δ::natNT2-TEF1pr-mCherry-CYC1term pdr5Δ::hphNT1	this study
yKBJ0201	yMaM1205 leu2Δ::natNT2-TEF1pr-mNeonGreen-CYC1term pdr5Δ::hphNT1	this study
yKBJ0202	yMaM1205 leu2Δ::natNT2-TEF1pr-mCherry-CYC1term pdr5Δ::hphNT1 pRS41K-3myc-HaloTag	this study
yKBJ0203	yMaM1205 leu2Δ::natNT2-TEF1pr-mNeonGreen-CYC1term pdr5Δ::hphNT1 pSD-N1-HaloTag-3myc	this study
yEG222	yMaM1205 lyp1Δ::GAL1pr-OsTIR1(F74G)-natMX	this study
AID-v1_OsTIR1^{-}_PDC1	MATa lyp1Δ his3Δ1 leu2Δ0 ura3Δ0 met15Δ0 can1Δ::STE3pr-LEU2-GAL1pr-NLS-I-SCEI PDC1-mNeonGreen-AID*-3myc-hph	this study
AID-v2_HIS4	MATa his3Δ1 leu2Δ0 ura3Δ0 met15Δ0 can1Δ::STE3pr-LEU2-GAL1pr-NLS-I-SCEI lyp1Δ::GAL1pr-OsTIR1(F74G)-natMX HIS4-AID*-3myc-hph	this study

Supplementary Table 7. Plasmids.

Plasmid	Description	Source
pSD-N1	CEN ARS kanMX (empty type I N-SWAT donor)	(Yofe et al., 2016)
pMaM482	pRS41K CEN ARS kanMX (empty type I C-SWAT donor)	(Meurer et al., 2018)
pEI098	pSD-N1-mNeonGreen (N-SWAT type I donor, tagging with mNeonGreen)	this study
pYD10	pRS41K-mNeonGreen (C-SWAT type I donor, tagging with mNeonGreen)	(Meurer et al., 2018)
pKBJ050	pSD-N1-HaloTag-3myc (N-SWAT type I donor, tagging with HaloTag-3myc)	this study
pKBJ051	pRS41K-3myc-HaloTag (C-SWAT type I donor, tagging with 3myc-HaloTag)	this study
pBL1099	pRS41K -AID*-3myc (C-SWAT type II donor, tagging with AID*-3myc)	this study
pBL1101	pRS41K-mNeonGreen-AID*-3myc (C-SWAT type II donor, tagging with mNeonGreen-AID*-3myc)	this study